

# Topological Information Embodied in Local Juxtaposition Geometry Provides a Statistical Mechanical Basis for Unknotting by Type-2 DNA Topoisomerases

Zhirong Liu<sup>1</sup>, Jennifer K. Mann<sup>2,3</sup>, E. Lynn Zechiedrich<sup>2,3</sup>  
and Hue Sun Chan<sup>1\*</sup>

<sup>1</sup>Department of Biochemistry  
and Department of Medical  
Genetics and Microbiology  
Faculty of Medicine  
University of Toronto, Toronto  
Ontario M5S 1A8, Canada

<sup>2</sup>Department of Mathematics  
Florida State University  
Tallahassee, FL 32306  
USA

<sup>3</sup>Department of Molecular  
Virology and Microbiology  
Baylor College of Medicine  
Houston, TX 77030, USA

Topoisomerases may unknot by recognizing specific DNA juxtapositions. The physical basis of this hypothesis is investigated by considering single-loop conformations in a coarse-grained polymer model. We determine the statistical relationship between the local geometry of a juxtaposition of two chain segments and whether the loop is knotted globally, and ascertain how the knot/unknot topology is altered by a topoisomerase-like segment passage at the juxtaposition. Segment passages at a “free” juxtaposition tend to increase knot probability. In contrast, segment passages at a “hooked” juxtaposition cause more transitions from knot to unknot than vice versa, resulting in a steady-state knot probability far lower than that at topological equilibrium. The reduction in knot population by passing chain segments through a hooked juxtaposition is more prominent for loops of smaller sizes,  $n$ , but remains significant even for larger loops: steady-state knot probability is only ~2%, and ~5% of equilibrium, respectively, for  $n=100$  and 500 in the model. An exhaustive analysis of ~6000 different juxtaposition geometries indicates that the ability of a segment passage to unknot correlates strongly with the juxtaposition’s “hookedness”. Remarkably, and consistent with experiments on type-2 topoisomerases from different organisms, the unknotting potential of a juxtaposition geometry in our polymer model correlates almost perfectly with its corresponding decatenation potential. These quantitative findings suggest that it is possible for topoisomerases to disentangle by acting selectively on juxtapositions with “hooked” geometries.

© 2006 Elsevier Ltd. All rights reserved.

**Keywords:** lattice model; exact enumeration; Monte Carlo sampling; conformational entropy; self-avoiding lattice polygon

\*Corresponding author

## Introduction

An understanding of the topology of covalently linked molecules<sup>1</sup> is important for the study of molecular biology.<sup>2</sup> For DNA, topological entanglements such as knots and catenanes can arise readily and frequently *in vivo*.<sup>3,4</sup> They are a natural biophysical consequence of conformational energetics and statistics.<sup>5</sup> The efficient resolution of DNA

entanglements is essential for proper cellular function. Topoisomerases perform this task by enabling DNA molecules to interconvert between different topological states. They accomplish this by catalyzing the passage of single-strand or double-helix DNA segments through each other via a transient breaking and subsequent resealing mechanism at a two-segment juxtaposition. These enzymes are involved in a wide range of cellular processes, including chromosome condensation and segregation, transcription, replication, and recombination.<sup>6,7</sup> In addition to their essential cellular roles, DNA topoisomerases are targets of many antibacterial and anticancer drugs.<sup>8–11</sup> Thus, fundamental insights into how topoisomerases function may lead to improved understanding of the medical ramifications as well.

Present address: H. S. Chan, Department of Biochemistry, University of Toronto, Medical Sciences Building-5th Fl., 1 King’s College Circle, Toronto, Ontario M5S 1A8, Canada.

E-mail address of the corresponding author:  
[chan@arrhenius.med.toronto.edu](mailto:chan@arrhenius.med.toronto.edu)

For many years since the discovery of the first topoisomerase,<sup>12</sup> it was widely believed that, besides DNA gyrase and reverse gyrase which introduce supercoiling, other topoisomerases resolve topological entanglements by converting a DNA molecule effectively into a phantom chain<sup>13</sup> that can seemingly defy excluded volume and freely pass through itself. It follows that the function of topoisomerases was largely seen as restoration and maintenance of a distribution of topological states approximating that at topological equilibrium.<sup>14–16</sup> In this context, it was surprising that type-2 topoisomerase, which changes DNA linking number in steps of two and passes segments of DNA double helix through each other in an ATP-dependent process, was discovered to be capable of lowering the steady-state levels of knots and catenanes well below their corresponding equilibrium values.<sup>17</sup> The size of a topoisomerase is substantially smaller than the DNA molecule on which it is acting. Thus, the experimental results of Rybenkov *et al.*<sup>17</sup> present a conceptual challenge: what information can the topoisomerase utilize to discriminate between different global topologies of the much larger DNA molecule? What dictates the topoisomerase's preference to act upon a particular DNA topology?

Several hypothetical scenarios have since been proposed to account for the apparent ability of type-2 topoisomerase to discriminate between different DNA topologies. Most of these proposals presume that local structural and energetic features of a pre-existing two-segment DNA juxtaposition do not contain enough information for a meaningful inference about the DNA molecule's global topological state. For example, one of the hypotheses proposes that the topoisomerase has to first actively deform the DNA conformation at the binding site to create a sharp turn; the bias towards unlinked and unknotted topology can then be realized by allowing only unidirectional DNA passage through this protein-induced turn.<sup>18,19</sup> Alternatively, other hypotheses endow topoisomerases with an ability to gather topological information beyond that which can be gleaned from a local juxtaposition, with mechanisms reminiscent of that for other cases of "action at a distance" in DNA enzymology.<sup>20</sup> Proposals in this category include a "three-binding-sites" model that states that the topoisomerase first binds and then actively slides along the DNA contour to find a third strand;<sup>17</sup> a "kinetic proofreading" model that requires two separate topoisomerase–DNA collisions for segment passage;<sup>21,22</sup> and a "three-segment interaction" model that stipulates enzyme–DNA interactions between a bound, essentially stationary topoisomerase with three DNA segments.<sup>23</sup> In common, all these hypotheses are "protein-centric." That is, the proposed activities of the type-2 topoisomerase prior to segment passage after its binding to the DNA are essential in creating new, probing information about global DNA topology. Then, the enzyme utilizes this new information that it has actively generated for selective segment passage (see Maxwell *et al.* for a recent review).<sup>24</sup>

A simpler hypothesis was put forth by Buck and Zechiedrich.<sup>25</sup> It stipulates that topological discrimination can be attained by considering only the local curvature of the two segments making up a juxtaposition and the resulting angle between them. Recognizing that DNA juxtapositions are preferred binding sites of type-2 topoisomerases<sup>25,26</sup> (and references therein), these authors proposed that a topoisomerase can sense the topological state of a DNA molecule and achieve disentanglement by selective segment passages only at pre-existing "hooked" but not "free" juxtapositions.<sup>25</sup> Recent structural data from X-ray crystallography appear to lend support to this view.<sup>27,28</sup> Additional biological data are also rationalized by this proposed scenario.<sup>29</sup>

From a theoretical perspective, we have devised a systematic statistical mechanical approach to assess the physical viability of this hooked *versus* free hypothesis.<sup>30</sup> Our outlook and method are "DNA juxtaposition-centric." Starting with a model of polymer chain conformations, we determine the distribution of topological states that are consistent with the existence of a preformed juxtaposition. We can then ascertain how segment passages at various juxtaposition geometries alter the topological states of the conformations.

As a first application of this methodology, we studied the topological states of catenation/decatenation<sup>31,32</sup> by considering the configurations of two loops (a pair of ring polymers) of various sizes. Using a coarse-grained lattice polymer model, we found that two-loop configurations with different juxtaposition geometries can have very different topological biases. In particular, an overwhelming majority of loops with a hooked juxtaposition are linked, whereas loops with a free juxtaposition are mostly unlinked. Consequently, segment passages at hooked juxtapositions tend to decatenate. In contrast, segment passages at free juxtapositions tend to catenate. As such, the topological discriminating power of a local juxtaposition is rather striking; and the discrimination remains significant even for loops of large sizes. These quantitative predictions are consistent with original estimates,<sup>25</sup> and are potentially critical for the applicability of the hypothesis to genome-size DNA. Physically, the model observations imply that different juxtaposition geometries impose different long-range topological biases. Although these biases are stronger for smaller loops than for larger loops, they cannot be erased by increasing loop size. Taken together, these results clearly established a statistical mechanical principle in polymer physics governing how local juxtaposition geometry is correlated with global topology. Thus, we have succeeded in demonstrating that the hooked *versus* free hypothesis is viable, at least for the two-loop catenation/decatenation case,<sup>30</sup> even though the detailed manner in which this principle may apply to real DNA molecules remains to be elucidated by further experimental and theoretical efforts.<sup>33</sup> Our previous study considered the linking/unlinking of two loops without regard to the various knot states of the individual

loops.<sup>30</sup> The results in that study correspond to conformational properties averaged over all possible knotted and unknotted two-loop configurations. As a natural next step of our investigation, and a crucial one for understanding DNA topology, here we apply our general approach to address questions of knotting and unknotting.<sup>17,34</sup>

As in our previous study, the present evaluation of the hooked *versus* free hypothesis consists of two main components.<sup>30</sup> In the first part of our effort, we determine the conformational populations of various knot states under equilibrium conditions. In particular, we are interested in how the relative equilibrium populations of knot *versus* unknot are affected by preformed juxtapositions of specific geometries. The methodology for computing the necessary conformational statistics is detailed in the next section. This part of our results provides an indispensable foundation for understanding juxtaposition-based topological discrimination, but it does not directly address the kinetic effects of type-2 topoisomerase action. In the second part of our modeling effort, we investigate directly the outcomes of topoisomerase-like segment passages at various juxtaposition geometries (see below). These model processes correspond to the ATP-driven activity of type-2 topoisomerases, and therefore implicitly involve an external energy source. Therefore, segment passage kinetics at selective juxtaposition geometries can lead to nonequilibrium situations, resulting in steady-state population distributions different from that at topological equilibrium.

## Counting Conformations in Various Knot States

We use lattice modeling for conformational statistics. Many of the details of this method and its background have been provided before.<sup>30</sup> In general, lattice modeling is a powerful investigative tool that has long been productive in many aspects of polymer physics<sup>35,36</sup> and biomolecular simulation.<sup>37</sup> In the past two decades, this coarse-grained approach has been applied extensively to the study of proteins,<sup>38–45</sup> for which topological entanglement appears to be rare.<sup>46–49</sup> During the same time, lattice models also have been used widely in the study of knots and various implications of topological entanglement in polymers, including many questions motivated by DNA topology. These efforts have made important advances.<sup>50–56</sup>

Here, we consider single-loop (one ring polymer) conformations configured on simple cubic lattices. Each conformation consists of  $n$  beads, and a set of  $n$  bonds joining the beads together to form a closed circuit, which can be knotted or unknotted. We refer to  $n$  as loop size. Each conformation is a self-avoiding polygon on the lattice, in that no two beads are allowed to occupy the same lattice site. In this model, every conformation is assigned the same statistical weight and thus effectively has the same energy, as in many elementary polymer and biomolecular models

of conformational statistics.<sup>57</sup> We do not consider temperature explicitly because the distribution of conformational states in the model is temperature-independent. Nonetheless, the assumption of ambient temperature allows conformations belonging to the same knot state to interconvert efficiently and establish thermodynamic equilibrium. Future work will augment the basic lattice polymer model with bending energies to study, for example, the interplay between persistence length and local DNA curvature.

The topological state (knot *versus* unknot) of each conformation is determined by evaluating the HOMFLY polynomial,<sup>58</sup> using a modified version of the algorithm of Jenkins†.<sup>59</sup> In addition to Jenkins' algorithm, we have also implemented type-1 and type-2 Reidemeister moves<sup>60</sup> to simplify each knot diagram before applying Jenkins' dynamic programming approach. For our simulations, this added procedure leads to very significant improvements in computational efficiency because many trivial crossings in the generated conformations can be removed by Reidemeister moves. We use exact enumeration<sup>30</sup> for small loop sizes,  $n \leq 30$ , to account exhaustively for all possible conformations. We are primarily interested in whether a conformation is knotted or unknotted‡, without regard to the topological complexity of the knotted conformations. It should be noted nonetheless that the computed HOMFLY polynomial of a conformation may be used to identify its knot type. Figure 1(a) and (b) provide example conformations of different knot types generated by our exact enumeration. In this figure and subsequent discussion, we adopt the knot-type notation of Rolfsen§,<sup>61</sup> and the customary practice of adding an asterisk (\*) if a given knot is the mirror image of the version in the Rolfsen table.

To assess the hooked *versus* free hypothesis in knotting/unknotting, we pay special attention to the five 5mer-on-5mer juxtapositions I, IIa, IIb, III, and IV in Table 1. The hooked (I), free planar (IIa and IIb), and free nonplanar (III) juxtaposition geometries are the same as those considered in our two-loop catenation/decatenation study.<sup>30</sup> Here, to broaden the analysis, we also consider the “half-hooked” juxtaposition (IV), because its geometry may be viewed as intermediate between that of the hooked and the free juxtapositions. Thus, an analysis of its properties can serve to elucidate how the topological discrimination power of a juxtaposition may depend on a more general measure of “hookedness.”

Geometrically, the half-hooked juxtaposition (IV) bears resemblance to a juxtaposition proposed by Vologodskii<sup>18</sup> as the specific local DNA geometry

† <http://www.burtleburtle.net/bob/knot/thesis.html>

‡ Mathematically, the unknot, which is also called the trivial knot ( $0_1$  in Figure 1(a)), refers to an unknotted circle. Accordingly, throughout this paper, “nontrivial knot” refers to a knotted circle.

§ <http://www.math.toronto.edu/~drorbn/KAtlas/Knots/index.html>

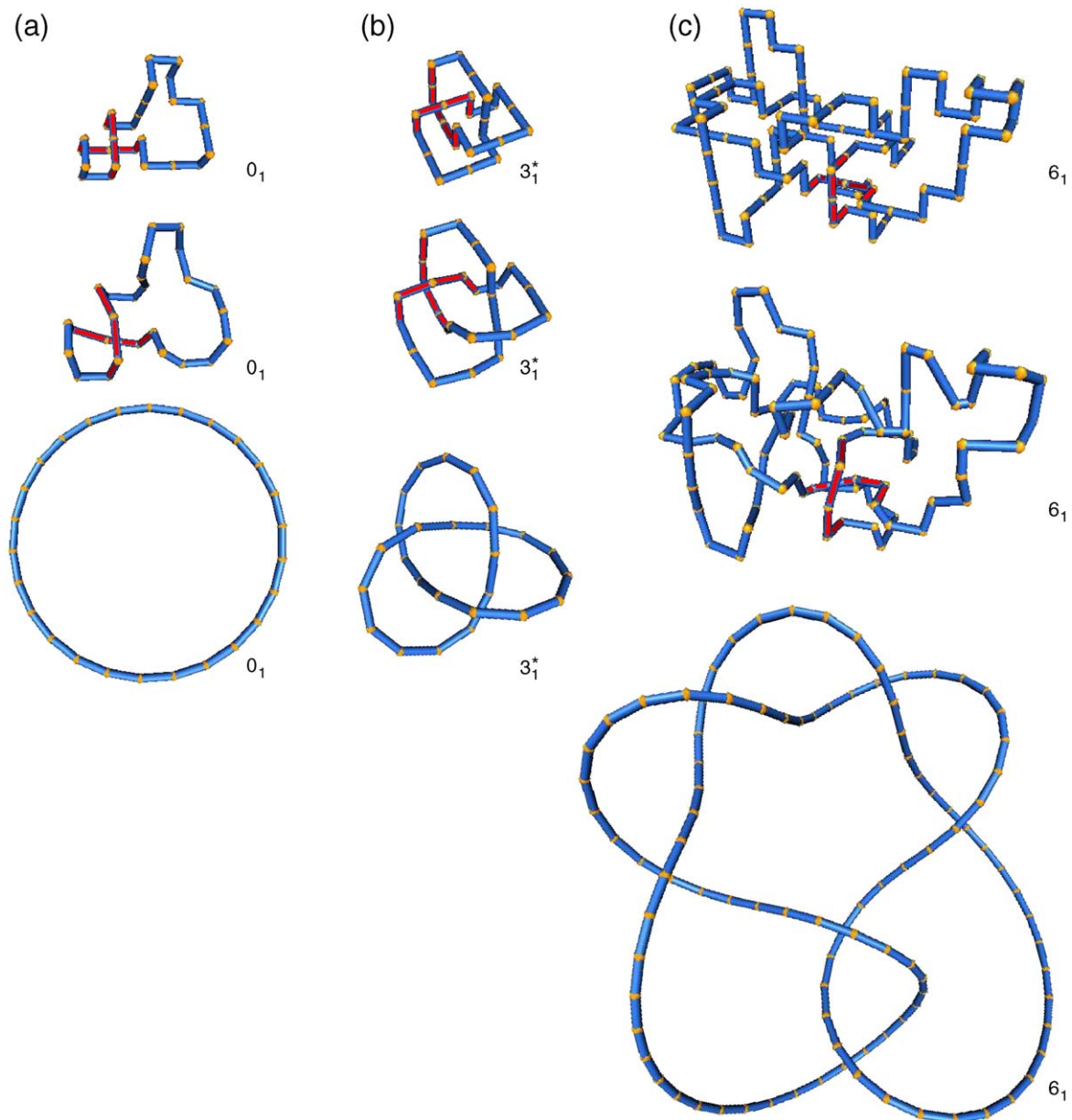


**Figure 1.** Examples of statistically mechanically generated unknot and knot conformations and results of smoothing the diagrams to remove extraneous crossings. (a) An unknot ( $0_1$ ) with loop size  $n=26$ , (b) a right-handed trefoil knot ( $3_1^*$ ) with loop size  $n=26$ , and (c) a 6-noded twist knot ( $6_1$ ) with loop size  $n=100$ . Top: Lattice conformations generated by exact enumeration (a, b) or Monte Carlo sampling (c). Middle: Intermediate smoothing diagrams of the conformations. Highlighted in red in each of these conformations is a hooked juxtaposition<sup>30</sup> (Table 1). Bottom: Minimal diagrams of top and middle for better visualization of the knot type. The KnotPlot program by R. G. Scharein was used in the preparation of this figure [<http://www.pims.math.ca/knotplot/>].

before segment passage by a type-2 topoisomerase. However, it should be noted that the underlying physical picture of this proposed topoisomerase mechanism<sup>18</sup> is different from the Buck-Zechiedrich hypothesis<sup>25</sup> because the curved segment is postulated to be actively introduced by the topoisomerase, rather than a pre-existing feature recognized by the enzyme. This will be discussed further below.

Looking beyond lattice model studies, we note that continuum (off-lattice) juxtaposition geometries may be classified using parameters constructed from generally defined geometric properties such as

tangent and curvature vectors of the pair of segments constituting the juxtaposition<sup>25,30</sup> (see below). For example, a recent atomic model study has investigated several hooked DNA juxtapositions with different segment curvatures.<sup>33</sup> Naturally, the likelihood of the occurrence of various juxtapositions in real DNA conformations as well as their topological discrimination power would be affected by local and global persistence lengths and other aspects of DNA conformational energetics. The impact of these physical factors on our proposed topoisomerase mechanism remains to be ascertained in future work.

**Table 1.** Number of one-loop conformations with a preformed juxtaposition, as a function of intersegment lengths  $n_1$ ,  $n_2$ , loop size  $n$ , and the knot type,  $K$ , of the conformation

$n_1, n_2, n$	$K$	I			IIa			IIb			III			IV		
		$0_1$	$3_1^*$	$0_1$	$0_1$	$3_1^*$	$3_1$	$0_1$	$3_1^*$	$0_1$	$3_1^*$	$4_1$	$0_1$	$3_1^*$	$4_1$	
2, 2, 14		1	0	0	0	0	0	0	0	1	0	0				
2, 4, 16		10	0	0	0	0	0	0	0	17	0	0				
2, 6, 18		143	0	0	0	0	0	0	0	243	0	0				
4, 4, 18		100	0	9	0	0	0	1	0	288	0	0				
2, 8, 20		2290	0	0	0	0	0	0	0	3682	0	0				
4, 6, 20		1428	0	354	0	0	0	60	0	4089	0	0				
2, 10, 22		38,111	0	0	0	0	0	0	0	59,466	0	0				
4, 8, 22		22,812	0	7493	0	0	0	1546	0	61,590	0	0				
6, 6, 22		20,175	0	13,436	624	0	0	3478	0	57,813	0	0				
2, 12, 24		657,334	0	0	0	0	0	0	0	1,003,092	0	0				
4, 10, 24		378,254	0	142,017	0	0	0	31,908	0	989,212	0	0				
6, 8, 24		319,528	0	282,778	19,828	0	0	88,558	0	867,176	0	0				
2, 14, 26		11,667,855	0	0	0	0	0	0	0	17,484,352	0	0				
4, 12, 26		6,495,772	0	2,627,920	0	0	0	625,173	0	16,607,211	96	0				
6, 10, 26		5,262,002	105	5,345,982	485,540	0	0	1,812,878	0	13,874,847	291	0				
8, 8, 26		5,023,674	130	5,933,887	584,866	0	0	2,246,453	0	12,962,184	162	0				
2, 16, 28		211,886,974	0	0	0	0	0	0	0	312,738,002	0	0				
4, 14, 28		114,782,354	0	48,679,426	0	0	0	12,091,399	0	288,308,860	4342	0				
6, 12, 28		89,831,165	3332	98,701,012	10,810,926	0	0	35,265,020	0	232,127,286	14,035	0				
8, 10, 28		82,247,146	11,270	111,913,553	13,720,982	0	0	45,819,223	0	206,760,342	12,579	0				
2, 18, 30		3,920,086,368	0	0	0	0	0	0	0	5,711,791,453	0	0				
4, 16, 30		2,075,378,380	0	909,145,466	0	0	0	233,679,565	0	5,139,175,837	128,615	0				
6, 14, 30		1,579,082,383	76,848	1,824,257,238	230,558,376	0	0	677,871,866	0	4,017,108,690	419,922	17				
8, 12, 30		1,397,138,914	356,412	2,061,511,670	297,822,258	40	40	888,025,330	48	3,449,645,239	481,017	3				
10, 10, 30		1,340,156,561	608,656	2,106,406,237	311,491,500	0	0	931,698,623	0	3,289,516,656	487,539	0				

We consider in detail 5mer-on-5mer hooked (I), free planar (IIa and IIb), free nonplanar (III), and half-hooked (IV) juxtapositions configured on the simple cubic lattice. The four endpoints of each juxtaposition are joined by self-avoiding lattice chains (represented by dashed curves) to complete a single-loop conformation;  $n_1$  and  $n_2$  are the lengths (numbers of beads) of the two connecting chains. For the free planar juxtaposition, the endpoints may be joined by either of two nonsymmetric connections yielding the juxtapositions IIa and IIb. Besides the free planar juxtaposition, each juxtaposition in this table consists of a single crossing. Following the sign convention of crossings in oriented knot diagrams, the crossing within juxtapositions I, III, and IV can be either positive (+) or negative (-). As the present study investigates interconversions between knot and unknot irrespective of nontrivial knot types, it is sufficient to consider only positive juxtapositions I, III, and IV, because, by symmetry, our main results are identical for the corresponding negative juxtapositions, as we have verified by explicit enumeration using juxtapositions of both signs for several loop sizes. For all juxtapositions considered in this work, the middle positions (beads) of the two segments making up the juxtaposition are nearest lattice neighbors, as highlighted by the dotted lines for the examples shown. The tabulated numbers are obtained by exact enumeration on simple cubic lattices. Each count corresponds to the number of self-avoiding polygons consistent with the existence of the given juxtaposition at a fixed position and orientation. The counts do not include any translational, rotational, or inversion transformation of the starting juxtaposition. In addition to the unknot ( $0_1$ ), both chiralities of the trefoil knot ( $3_1$  and  $3_1^*$ ), and the figure eight knot ( $4_1$ ) are encountered by the enumeration reported in this table. The numbers of beads  $n_1$  and  $n_2$  of the two connecting chains are related by  $n = n_1 + n_2 + n^{(j)}$ , where  $n^{(j)}$  is the number of beads in the juxtaposition;  $n^{(j)} = 10$  for I, IIa, IIb, III, and IV. Because of the geometric symmetry of these juxtapositions, the conformational count for  $n_1$  is identical with that for  $n - n^{(j)} - n_1$ . Thus, only counts for  $n_1 = 2, 4, \dots, (n - n^{(j)}) / 2$  are provided.

As stated above, the starting point of our analysis is a preformed juxtaposition. In this respect, our methodology is distinct, yet complementary to other coarse-grained modeling investigations of polymer entanglement.<sup>50–56,62–71</sup> Here, for a range of small loop sizes, Table 1 gives the exact numbers of conformations that resulted from each of these five preformed juxtapositions. Each count in the table corresponds to the number of one-loop conformations with at least one instance of the given juxtaposition. These exact counts are obtained by “growing” from an end of one of the two segments within a preformed juxtaposition, and the growing chain is

constrained to join to one end of the other segment as required by the orientation induced by either the sign (for I, III, and IV) or segment directions (for IIa and IIb) of the juxtaposition (Table 1). For juxtapositions I, III, and IV, we consider only juxtapositions with a positive crossing. In these three cases, the requirement of a positive crossing mandates how the growing chain connects to the other segment. In the case of juxtapositions IIa and IIb, there is no crossing, but there are two distinct ways (a and b) for the growing chain to connect to the other segment.

Conformations of larger loops are generated by Monte Carlo sampling. Our simulation procedure

combines the Madras *et al.* (MOS)<sup>72</sup> and BFACF<sup>73,74</sup> algorithms. We have demonstrated that the MOS algorithm is efficient for sampling two-loop configurations with a preformed juxtaposition between the loops.<sup>30</sup> However, for the present one-loop system, MOS is insufficient to sample all possible conformations because the MOS chain moves do not change the lengths of the connecting chains ( $n_1, n_2$  in Table 1), but conformations with different ( $n_1, n_2$ ) values can be consistent with a given juxtaposition. To overcome this problem, we now also include the BFACF chain move<sup>73,74</sup> that changes loop size (number of beads) by 2. With this additional move, variation of ( $n_1, n_2$ ) can be realized by first shortening one of the connecting chains, resulting in, for example, ( $n_1-2, n_2$ ). In a subsequent step, the other connecting chain can be elongated, which would then result in ( $n_1-2, n_2+2$ ). We further restrict the procedure so that it only samples conformations of specific loop sizes: for any loop size  $n$  we choose to study, BFACF moves that lead to a larger loop size are forbidden when the loop size is  $n$ , and BFACF moves that lead to a smaller loop size are forbidden when the loop size is  $n-2$ . Hence, only loop sizes  $n$  and  $n-2$  are sampled by our algorithm, and conformational/topological properties of interest can be computed separately for  $n$  and  $n-2$ . The above described combination of MOS and BFACF moves achieves ergodicity in our simulation.

With the BFACF move in place, our overall Monte Carlo procedure, which maintains detailed balance (an unbiased conformational exploration), is as follows. Starting with any one-loop conformation, a stochastic decision is first made to use either the BFACF move or the MOS moves. Let the probability of choosing the BFACF move be  $p_n(-2)$  if loop size= $n$ , and  $p_{n-2}(+2)$  if loop size= $n-2$ . The corresponding probabilities of choosing the MOS moves are, respectively,  $1-p_n(-2)$  or  $1-p_{n-2}(+2)$ . If a decision to use MOS is made, a pair of beads within the same connecting chain, as well as the two endpoints of the juxtaposition segments attached to the given connecting chain, are chosen randomly with uniform probability, and the same MOS procedure as described in our previous study<sup>30</sup> is applied to generate a putative new conformation. If a decision to use BFACF is made, a bead position,  $i$ , is chosen randomly with uniform probability, irrespective of whether the bead is part of the preformed juxtaposition. Then, to generate a putative new conformation, if loop size= $n$ , a BFACF move is used to delete two beads between  $i$  and  $i+3$ ; if loop size= $n-2$ , a BFACF move is used to add two extra beads between  $i$  and  $i+1$  with uniform probability for the four possible pairs of lattice positions for the extra beads. After a putative conformation is produced from either the MOS or BFACF move, that move is accepted if the new conformation does not violate excluded volume and does not alter the preformed juxtaposition. Otherwise, the move is rejected and the original unchanged conformation contributes one more time to the sample.

The procedure described above was carried out for a wide range of loop sizes (from  $n=20$  to  $n=500$ ), with various preformed juxtapositions, using  $p_n(-2)=p_{n-2}(+2)=0.01$ . Our BFACF sampling is efficient. For the largest loop size we have simulated ( $n=500$ ), the ratios of the number of accepted BFACF moves (transitions between loop sizes  $n$  and  $n-2$ ) to the total number of attempted BFACF moves were  $\sim 0.145, 0.156, 0.158, 0.157$ , and  $0.157$ , respectively, for the hooked (I), free planar (IIa and IIb), free nonplanar (III), and half-hooked (IV) juxtapositions. A representative knotted conformation generated by this Monte Carlo procedure is given in Figure 1(c). Although the Monte Carlo procedure – unlike exact enumeration – is not exhaustive, a wide range of knot states was sampled. For example, the number of different HOMFLY polynomials (knot types) encountered in our  $n=500$  simulation is 24 when no juxtaposition was preformed. The corresponding number of knot types sampled, 51, is much higher for  $n=500$  loops with a preformed hooked juxtaposition (I).

We have performed a self-consistency check by verifying that results from Monte Carlo sampling of small loops are in excellent agreement with results from exact enumeration. To check that the HOMFLY knot/unknotted determination algorithm was implemented correctly, we have chosen  $>150$  conformations of various loop sizes and verified, by visual inspection, that conformations determined to have HOMFLY polynomials  $P(l, m)=1$  are unknotted, and those determined to have  $P(l, m)\neq 1$  are knotted. Further checking was conducted by evaluating the Alexander polynomials<sup>75</sup> for  $\sim 7000$  of the generated conformations using the algorithm of Harris and Harvey<sup>76</sup>. For our diverse set of conformations, we verified that the knot types determined by the HOMFLY algorithm are consistent with that determined by the Alexander polynomial algorithm, aside from the fact that the Alexander polynomial cannot distinguish a knot from its mirror image.

## Results and Discussion

### Conformational counts and knot probabilities

We begin by examining the effects of various preformed juxtapositions on the probability,  $p_K$ , that a one-loop conformation is knotted. For unconstrained one-loop conformations, it has long been known that  $p_K$  increases with loop size.<sup>50,77</sup> Experimental results agree.<sup>5,17</sup> For self-avoiding but otherwise unconstrained loops configured on the simple cubic lattice,  $n=24$  is the minimum loop size that allows a knot (a trefoil) to be formed.<sup>78</sup> Consistent with the general trend, the exact counts in Table 1 show that, for small loops, the fractions of conformations that are knotted are very small.

However, although  $p_K$  is small for all five preformed juxtaposition geometries considered, the differences in  $p_K$  among them are striking. Take  $n=30$  for example, after summing up conformational counts for all possible  $n_1, n_2$ , the knot probability  $p_{K|j}$  conditioned upon a given preformed juxtaposition  $j$  are  $p_{K|I}=1,475,176/19,285,003,827=7.6 \times 10^{-5}$ ,  $p_{K|IIa}=0$ ,  $p_{K|IIb}=160/1,368,252,928=1.2 \times 10^{-7}$ ,  $p_{K|III}=96/4,530,852,241=2.1 \times 10^{-8}$ , and  $p_{K|IV}=2,546,687/39,927,505,781=6.4 \times 10^{-5}$ . In other words, for this loop size, if a hooked (I) or half-hooked (IV) juxtaposition is observed, the conditional probability that the underlying conformation is knotted is at least two to three orders of magnitude higher than that if one of the free juxtapositions (IIa, IIb, III) is observed instead. This behavior implies that substantial topological information regarding knotting is embodied in local juxtaposition geometry. It points to the likelihood that segment passages at specific juxtaposition geometries can lead to significant topological biases. Intuitively, segment passage at a hooked juxtaposition (I) would result in a free nonplanar juxtaposition (III), and vice versa. Thus, the lower  $p_{K|j}$  for loops with a juxtaposition III than that with a juxtaposition I suggests that segment passage at a hooked juxtaposition would tend to unknot.

Figure 2 shows knot probabilities over a wider range of loop sizes for unconstrained loops (without preformed juxtapositions) and for loops with preformed juxtapositions: hooked (I), free planar (IIa, IIb), free nonplanar (III), or half-hooked (IV). For  $n=500$  unconstrained loops,  $p_K=0.00174$ , which agrees with the previously determined value of  $0.00151 \pm 0.00028$ .<sup>53</sup> The knot probability for loops

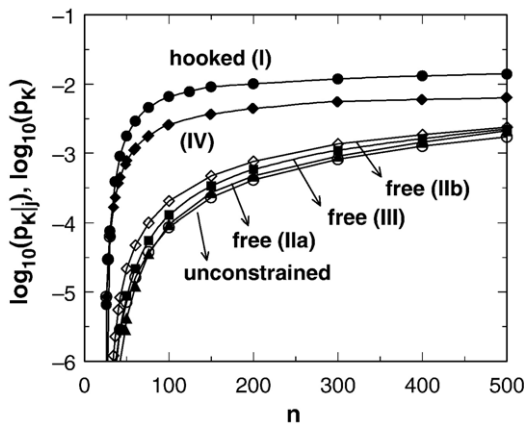


**Figure 2.** Dependence of knot probability,  $p_{K|j}$ , on loop size  $n$ , for conformations with a preformed hooked (I, ●), free planar (IIa, ▲; or IIb, ◇), free nonplanar (III, ■), or half-hooked (IV, ◆) juxtaposition. Corresponding knot probabilities,  $p_K$ , for loops with no preformed juxtaposition, or unconstrained (○), are included for comparison. Exact enumeration was used for juxtapositions I, IIa, IIb, III, and IV for  $n \leq 30$ , and also IIb for  $n=32$ , and for unconstrained loops for  $n \leq 20$ . Knot probabilities for larger  $n$  values were computed by Monte Carlo sampling, with the number of attempted chain moves for each datapoint varying from  $6 \times 10^9$  to  $2 \times 10^{10}$ .

with a hooked juxtaposition (I) is higher than that with a half-hooked juxtaposition (IV) (for example,  $p_{K|I}=0.0139$  and  $p_{K|IV}=0.00683$  for  $n=500$ ), even though the half-hooked juxtaposition generates more knots and samples more knot types for small loops (Table 1). The most likely explanation for the increased number of knots and increased knot complexity is that the half-hooked juxtaposition places less restriction on conformational freedom.

From our perspective, the most important message from Figure 2 is that knot probability of loops with either a hooked or a half-hooked juxtaposition is significantly higher than that with any one of the free juxtapositions, which is similar to the unconstrained case. This topological discriminating power of the juxtapositions is most prominent for smaller loop sizes. As anticipated,<sup>25,30</sup> the effect diminishes somewhat for larger loops, but it remains significant for loops as large as  $n=500$ .

Intuitively, the topological bias resulting from preformed juxtapositions may be understood as follows. If one considers a preformed hooked juxtaposition, it is quite obvious that the intertwinning of the two segments of the hooked juxtaposition tends to increase the probability of entanglement. If the loop size is small, this bias is strong because total loop length is insufficient for the chains emanating from the preformed juxtaposition to both “turn around” to undo the initial topological bias and at the same time close the loop to form a ring polymer. The trend resulting from this severe constraint is clear from the exact enumeration data in Table 1. For larger loops, it is possible for the chains emanating from the preformed juxtaposition to accomplish both. This accounts for the fact that the corresponding topological biases are less prominent than that for smaller loops. Nonetheless, no matter how long the total loop length, several bond and torsion angles have to be restricted before the chains can establish new growing points that are essentially free of the constraining effects of the preformed juxtaposition. Thus, conformational entropy would be lost. This consideration suggests that no matter how large the loop size, the topological biases of certain preformed juxtapositions cannot be entirely abolished, a trend that appears to have been borne out in the data shown in Figure 2.

### Juxtaposition geometries and knot/unknot discrimination

The trend in Figure 2 may be understood in a wider context by considering all possible 5mer-on-5mer juxtapositions and by characterizing juxtaposition geometries, as done previously,<sup>30</sup> using the dot (scalar) product  $\vec{N}_1 \cdot \vec{N}_2$  of the curvature vectors  $\vec{N}_1, \vec{N}_2$  of the two segments that comprise a given juxtaposition, and what we call the “hook parameter”  $H$  defined by:

$$H = \vec{N}_1 \cdot \vec{r}_{12} + \vec{N}_2 \cdot \vec{r}_{21} \quad (1)$$

where  $\vec{r}_{12}, \vec{r}_{21}$  are the vectors between the two central positions of the two segments of the juxtaposition (Figure 3(a)). Our choice of using 5mer-on-5mer juxtapositions represents a practical balance between two modeling requirements: computational tractability and a sufficient coverage of subtle geometrical effects that can only be captured by lattice chain segments with more beads. By construction, the sign of  $H$  depends on whether the two segments of the juxtaposition are hooked towards each other ( $H > 0$ ) or curved away from each other ( $H < 0$ ), such that  $H$  may be viewed as a measure of the hookedness of the juxtaposition. The correspondence is particularly apparent when the curvature vectors  $\vec{N}_1$  and  $\vec{N}_2$  are pointing away from each other ( $\vec{N}_1 \cdot \vec{N}_2 < 0$ ). In that case, when the two segments are intertwined like a hook, the curvature vector  $\vec{N}_1$  of the first segment tends to be aligned positively with the direction of the vector  $\vec{r}_{12}$  from the central bead of the first segment to the central bead of the second segment, resulting in a positive value for the dot product  $\vec{N}_1 \cdot \vec{r}_{12}$  [first term in equation (1)]. The same consideration applies to the curvature vector  $\vec{N}_2$  of the second segment and the vector  $\vec{r}_{21}$  [second term in equation (1)]. Thus, an intuitive sense of hookedness clearly increases for more positive values of  $H$ , with the hooked juxtaposition (I) reaching the maximum value of

$H = 2$ . By a similar consideration, it can be seen that more negative values of  $H$ , on the other hand, are associated with increasing geometric similarity to the free juxtapositions IIa, IIb, or III, which take the minimum value of  $H = -2$ .<sup>30</sup>

A total of 2982 distinguishable 5mer-on-5mer juxtapositions were considered for the two-loop study.<sup>30</sup> The count of distinguishable 5mer-on-5mer juxtapositions in the present study of one-loop conformations is different from that of two-loop conformations. For two-loop catenation/decatenation, the two segments belong to two different loops. In that case, the contour direction of each segment can be reversed without affecting the connectivity pattern. Thus, juxtapositions related by reversing the contour direction of one but not both segments were taken to be equivalent. In contrast, one-segment reversals in the one-loop case have to be treated as intrinsically distinct because they represent different connectivity patterns, as exemplified by the different knot probabilities for juxtapositions IIa and IIb (Table 1). It follows that the number of distinguishable juxtapositions should be approximately double that in the two-loop study. The number of 5mer-on-5mer juxtapositions on the simple cubic lattice that cannot be transformed into one another by translation, rotation, inversion, swapping of the two segments, or reversing the

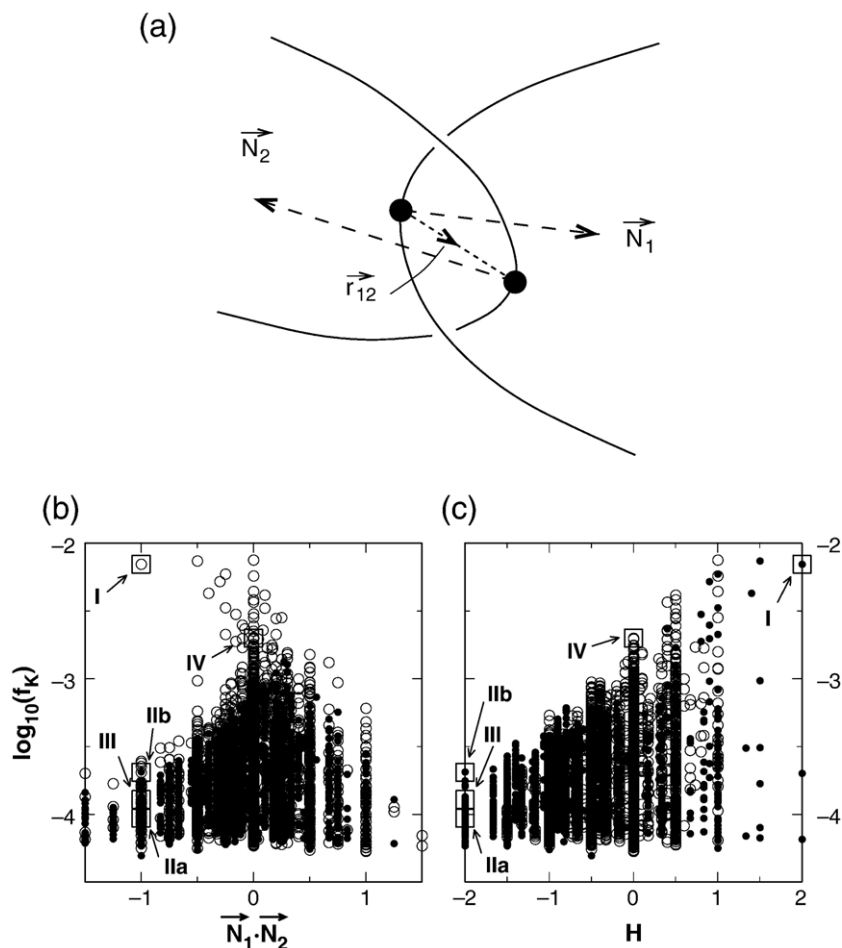


**Figure 3.** (a) Schematic of an analytical description of juxtaposition geometry.  $\vec{N}_1$  and  $\vec{N}_2$  are the curvature vectors of the two chain segments that make up a given juxtaposition, while  $\vec{r}_{12} (= -\vec{r}_{21})$  is the vector between the central positions of the two segments.<sup>30</sup> (b, c) Correlation between global knot/unknot topology and local juxtaposition geometry. The knot/unknot discrimination factor,  $f_K$ , of all 5899 possible 5mer-on-5mer juxtapositions for loop size  $n = 100$  was determined by Monte Carlo simulations using  $1 \times 10^8$  attempted chain moves for each datapoint. (b) Scatter plots for  $\vec{N}_1 \cdot \vec{N}_2$ , where (O) and (●) represent, respectively, juxtapositions with  $H \geq 0$  and  $H < 0$ . (c) Scatter plots for  $H$ , where (O) and (●) represent, respectively, juxtapositions with  $\vec{N}_1 \cdot \vec{N}_2 \geq 0$  and  $\vec{N}_1 \cdot \vec{N}_2 < 0$ . Large squares with arrows marked by I, IIa, IIb, III, and IV are, respectively,  $f_K$  values for the hooked juxtaposition, the three free juxtapositions, and the half-hooked juxtaposition in Table 1.

contour directions of both segments is 5899. This number is very nearly  $2 \times 2982 = 5964$ . The two numbers are not exactly equal because, for a small number of highly symmetric juxtapositions such as juxtapositions I and III, reversing the contour direction of one, but not the other segment only yields an equivalence of the original juxtaposition.

Figure 3(b) and (c) examines the knot/unknotted discrimination factor,  $f_K$ , of all 5899 5mer-on-5mer juxtapositions. Similar to the linked/unlinked discrimination factor,  $f_L$ , we defined previously,<sup>30</sup> the factor  $f_K = (p_K|j) / (p_U|j) = (p_K|j) / (1 - p_K|j)$  is the ratio of knot to unknot probabilities. It quantifies the information encapsulated in a local juxtaposition  $j$  about the global knot/unknotted state of the entire one-loop conformation. Similar to the corresponding results in the catenation/decatenation study (Figure 9 of Liu *et al.*),<sup>30</sup> the scatter plots in Figure 3 provide the variation of  $f_K$  with respect to the geometrical characteristics of a juxtaposition. Figure 3 shows that even for a relatively large loop size  $n = 100$ , the variation of  $f_K$  is extensive. Although all  $f_K$  values plotted are small ( $\ll 1$ ) because knot probabilities are generally low for the loop sizes we have examined (Figure 2), the  $f_K$  values for different juxtapositions can differ by more than two orders of magnitude, indicating that local juxtaposition geometry provides significant discrimination about whether the conformation is globally knotted.

The diversity in  $f_K$  decreases with increasing absolute value of  $\vec{N}_1 \cdot \vec{N}_2$ , except for a few  $\vec{N}_1 \cdot \vec{N}_2 \leq 0, H \geq 0$  juxtapositions (open circles in Figure 3(b)). The spread increases with  $H$  (Figure 3(c)). The minimum  $f_K$  value is not sensitive to either  $\vec{N}_1 \cdot \vec{N}_2$  (Figure 3(b)) or  $H$  (Figure 3(c)). Notably, however, the maximum  $f_K$  value is strongly correlated with the hook parameter  $H$ . Generalizing the trends in Figure 2, higher knot probabilities are seen here as associated with juxtaposition geometries with positive hookedness ( $H > 0$ ) and curvature vectors that tend to point away from each other ( $\vec{N}_1 \cdot \vec{N}_2 \leq 0$ ). The hooked juxtaposition (I) and the free nonplanar juxtaposition (III) are either at or near the two extremes of the spectrum of  $f_K$  values. Consistent with the knot probability trend discussed above, the  $f_K$  value for III is lower than that of the free planar juxtaposition (IIb), but is higher than that of the free planar juxtaposition (IIa). As expected from its half-hooked geometry and consistent with Figure 2, the behavior of juxtaposition IV is intermediate between that of the hooked and free juxtapositions.

### Segment passage and steady-state distribution of topoisomers

The strong dependence of a juxtaposition's topological biases on its geometry, under equilibrium conditions considered above, suggests that the outcome of segment passage at juxtapositions with different geometries could also be different. Now, to study directly the nonequilibrium kinetics of type-2 topoisomerase-like unknotting, we analyze segment

passages at juxtapositions of various geometries. We use "virtual" segment passage operations<sup>30</sup> to change the sign of a crossing. The procedure is depicted schematically in Figure 4. These hypothetical operations are designed to change the local geometry of the juxtaposition while leaving the rest of the conformation and its overall shape intact. One possible way to achieve this, as introduced in our previous study,<sup>30</sup> is to swap the positions of the two center beads, one on each of the two segments of a juxtaposition, and subsequently reroute the chain through the pair of exchanged positions, as in Figure 4(a). Here, to cover a broader range of possible local actions of a type-2 topoisomerase, we consider a generalization of this procedure, whereby a segment passage is defined by changing the sign of the crossing of a juxtaposition, provided the juxtaposition has a crossing. This generalized procedure includes the previously defined operation of swapping only one bead from each segment, but it can also entail swapping the positions of two or three (but not more) beads on each segment, which effectively changes the positions of four or six beads (Figure 4(b) and (c)). We refer to these segment-passage operations as virtual because they are only executed conceptually to calculate the resulting change, or lack thereof, of the knot state of the conformation, without our being concerned that the product conformation is not configured entirely on the simple cubic lattice. We simply invert juxtapositions to determine the global topological outcome, which may, in theory, mimic type-2 topoisomerase activity.

Not all juxtaposition geometries in our model can undergo type-2 topoisomerase-like segment passages. Many lattice juxtapositions lack a crossing, because substantial fractions of the two segments are parallel or lying on the same plane.<sup>30</sup> As a result, they do not permit virtual segment passage operations (Figure 4(d)). Among the 5899 5mer-on-5mer juxtapositions, 680 have a crossing that can undergo segment passage. Out of these 680 juxtapositions, 175 can undergo segment passage by swapping two beads, one bead from each segment of the juxtaposition (Figure 4(a)), whereas 505 juxtapositions can undergo segment passage by swapping four or six beads (Figure 4(b) and (c)). Hence, in the discussion below, for the purpose of exploring ramifications of our model predictions for type-2 topoisomerase action, we focus only on these two restricted sets of juxtapositions.

Type-2 topoisomerases can drive the DNA conformational ensemble away from equilibrium<sup>18,19</sup> if their action is sensitive to DNA local geometry such that segment passage is effected only at one particular juxtaposition geometry (or a selective set of juxtaposition geometries), but not others. In other words, local geometric selectivity of type-2 topoisomerases can result in a shift in the steady-state knot/unknot conformational distribution, and their ATP-driven enzymatic action can maintain a distribution different from that at a topological equilibrium.

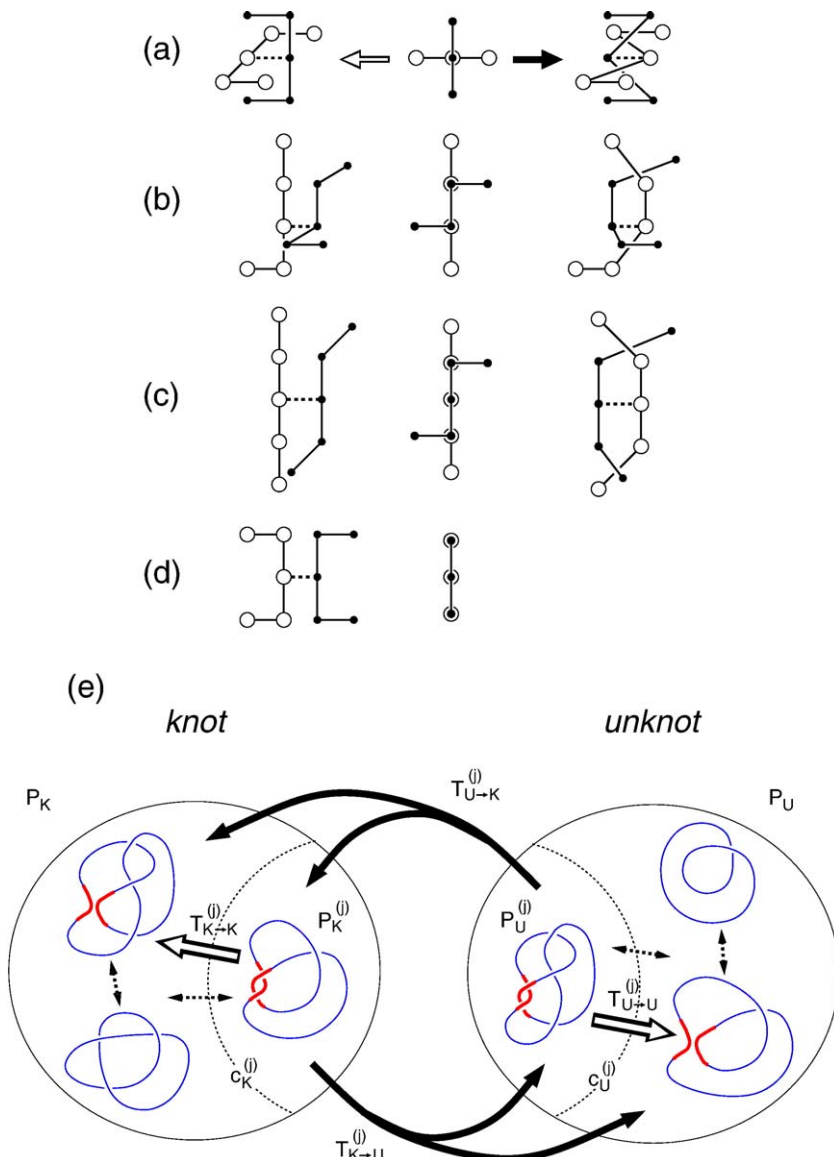


**Figure 4.** Modeling nonequilibrium kinetic effects of segment passage. (a)–(d) Virtual segment passage at various juxtapositions. The transformations depicted here mimic type-2 topoisomerase activity, and thus require energy input implicitly. These local conformational changes are distinct from, and not part of the chain moves used in the Monte Carlo equilibrium sampling. In (a)–(d), beads on the two segments of a juxtapositions are depicted as open circles and solid dots for clarity. Left: Examples of original juxtaposition geometries before segment passage. Right: Corresponding juxtaposition geometries after virtual segment passage. Middle: Projection of the juxtaposition before segment passage in the left-pointing direction indicated by the hollow arrow. The middle projection is identical with that of the juxtaposition after segment passage in the right-pointing direction indicated by the solid arrow. For juxtaposition I in (a), virtual segment passage may be defined as exchanging the central bead in each of the two segments. For the juxtapositions in (b) and (c), virtual segment passage is defined as swapping the positions, respectively, of two and three inside beads in each of the two segments. There is one, and only one, crossing in the projection diagram in each of the examples in (a), (b), and (c). The sign of this crossing changes upon virtual segment passage. However, for the example in (d), which represents both juxtaposition Ia and Ib, there is no crossing in the projection diagram and, thus, virtual segment passage is not allowed. It may be noted that the

schematic drawings of juxtaposition configurations after segment passage (Right) resemble conformations in certain bond fluctuating models,<sup>65</sup> but not that in our simple cubic lattice model. This illustrative feature is of no concern to our analysis<sup>30</sup> because these segment-passage operations are only virtual (see the text). (e) Schematic for the analysis of the change in steady-state knot/unknot population ratio as a result of segment passage at a given juxtaposition. The total population of knot and unknot conformations are represented by the left and right big circles. Flow between the two topologically distinct populations (thick, solid arrows) is assumed to be possible only via segment passages at a given juxtaposition geometry  $j$  (illustrated by hooked juxtapositions, in red). Accordingly, the flow can only occur for a subpopulation  $P_K^{(j)}$  of the knot conformations and a subpopulation  $P_U^{(j)}$  of the unknot conformations, which are separated schematically from the rest by dotted demarcations. Conformations may interconvert freely within the knot population (increasing or decreasing knot complexity) and likewise within the unknot population (as indicated by the dotted arrows), such that the fractions of conformations with the juxtaposition  $j$  in these two populations,  $c_K^{(j)} = P_K^{(j)}/P_K$  and  $c_U^{(j)} = P_U^{(j)}/P_U$ , are constants. Segment passages can also leave the knot state of a conformation unchanged (large hollow arrows); the corresponding knot to knot and unknot to unknot transition probabilities are denoted by  $T_{K \rightarrow K}^{(j)}$  and  $T_{U \rightarrow U}^{(j)}$ .

We now model scenarios of enzymatic kinetics in which segment passage is only allowed at one particular juxtaposition geometry. Our goal is to determine how the resulting segment passage-induced change in the relative knot/unknot population depends upon juxtaposition geometry. Figure 4(e) summarizes our formulation. It shows the kinetic connectivities among various topological states (which pairs of states can interconvert

directly) and how their populations are governed by a set of transition rates. This modeling approach to population dynamics is often referred to as a master equation method.<sup>79,80</sup> Here, we use  $P_K$  and  $P_U$  to represent, respectively, the knot and unknot conformational populations. Under the condition that these populations can only be changed by segment passages at a specific juxtaposition geometry,  $j$ , and the simplifying assumption that the rate

of segment passage is independent of the position of the juxtaposition and overall loop conformation, the rate of change of  $P_K$  with respect to time,  $t$ , is given by:

$$\frac{dP_K}{dt} = b \left( P_U^{(j)} T_{U \rightarrow K}^{(j)} - P_K^{(j)} T_{K \rightarrow U}^{(j)} \right) \quad (2)$$

where  $P_U^{(j)}$  and  $P_K^{(j)}$  are, respectively, the unknot and knot conformational populations with at least one instance of juxtaposition  $j$  in each conformation. The quantity  $T_{U \rightarrow K}^{(j)}$  is the transition probability that, given that the initial conformation is an unknot, segment passage at the juxtaposition changes it to a knot; similarly,  $T_{K \rightarrow U}^{(j)}$  is the transition probability that, given that the initial conformation is a knot, segment passage at the juxtaposition changes it to an unknot; and  $b > 0$  is a constant that sets the time scale of our model system and effectively converts these transition probabilities to transition rates. Equation (2) states that the rate of change of total knot population (left side) is equal to the rate of gain in knot population from unknot population (first term on the right side) minus the rate of loss in knot population to unknot population (second term on the right side). Because of population conservation,  $P_K + P_U$  is constant. Thus, once a solution for  $P_K$  is obtained from equation (2),  $P_U$  is also known.

Assuming that unknot and knot conformations can, within their separate ensembles, equilibrate thermally (Figure 4 and discussion below)<sup>¶</sup>, the unknot and knot populations with at least one juxtaposition  $j$  are, respectively, given by  $c_U^{(j)} P_U$  and  $c_K^{(j)} P_K$ . Equation (2) may then be rewritten as:

$$\frac{dP_K}{dt} = b \left( c_U^{(j)} P_U T_{U \rightarrow K}^{(j)} - c_K^{(j)} P_K T_{K \rightarrow U}^{(j)} \right) \quad (3)$$

Because the steady-state unknot and knot populations,  $(P_U)_{st}$  and  $(P_K)_{st}$ , respectively, satisfy the equation:  $dP_K/dt=0$ , it follows from equation (3) that:

$$c_U^{(j)} (P_U)_{st} T_{U \rightarrow K}^{(j)} = c_K^{(j)} (P_K)_{st} T_{K \rightarrow U}^{(j)} \quad (4)$$

The terms in the above expression, equation (4), are readily related to quantities obtained from our model computation. Using the methods described above, our juxtaposition-centric simulations determine directly the probabilities of knot to unknot and unknot to knot transition via segment passage at a

given juxtaposition geometry. Let these directly simulated probabilities, which are normalized by all segment-passage events, be denoted, respectively, by  $\mathcal{J}_{K \rightarrow U}^{(j)}$  and  $\mathcal{J}_{U \rightarrow K}^{(j)}$ . By definition:

$$T_{K \rightarrow U}^{(j)} = \frac{\mathcal{J}_{K \rightarrow U}^{(j)}}{(P_K)_{eq}^{(j)}} = \frac{\mathcal{J}_{K \rightarrow U}^{(j)}}{c_K^{(j)} (P_K)_{eq}} \quad (5)$$

where  $(P_K)_{eq}^{(j)}$  and  $(P_K)_{eq}$  are, respectively, the knot population under conditions of topological equilibrium with and without the constraint of having at least one instance of the given juxtaposition geometry  $j$ . In equation (5), these quantities are normalized by the total knot and unknot population, thus they correspond, respectively, to the  $p_{K|j}$  and  $p_K$  values in Figure 2 with and without the constraint of a preformed juxtaposition. A similar equation applies for the  $U \rightarrow K$  transition<sup>a</sup>.

Hence, combining equation (4) and equation (5):

$$\frac{(P_U)_{st}}{(P_K)_{st}} = R_K \frac{(P_U)_{eq}}{(P_K)_{eq}} \quad (6)$$

where

$$R_K = \frac{\mathcal{J}_{K \rightarrow U}^{(j)}}{\mathcal{J}_{U \rightarrow K}^{(j)}} \quad (7)$$

is the knot reduction factor that depends on juxtaposition geometry ( $j$ ). This factor quantifies how much the steady-state unknot/knot population ratio is increased by segment passages relative to the corresponding equilibrium ratio, and can be compared with experimental measurements.<sup>17</sup> It is noteworthy that factors of  $c_U^{(j)}$ , and of  $c_K^{(j)}$ , cancel in equation (6), such that the knot reduction factor can be obtained in our formulation without knowledge of the equilibrium unknot/knot population ratio  $(P_U)_{eq}/(P_K)_{eq}$ .

We should point out that the above formulation is an approximation in the sense that segment passage-induced transitions between trefoils and more complex knot types in the  $P_K$  ensemble are not taken into consideration in the determination of  $R_K$ , because our treatment entails only a binary choice between an unknot state and a knot state. In principle, juxtaposition-mediated transitions between different nontrivial knot types can be modeled by a general master equation formalism that accounts for more than two conformational states.<sup>79,80</sup> Nonetheless, we have taken a simpler

<sup>¶</sup> The present treatment assumes a finite temperature. Physically, equation (2) assumes that thermal equilibration of conformations within the knot or unknot state is fast compared to the rate of type-2 topoisomerase-mediated segment passage. Transitions between the knot and unknot states can only be achieved by type-2 topoisomerase-mediated segment passage, i.e., there is no thermal equilibration between the knot and unknot states.

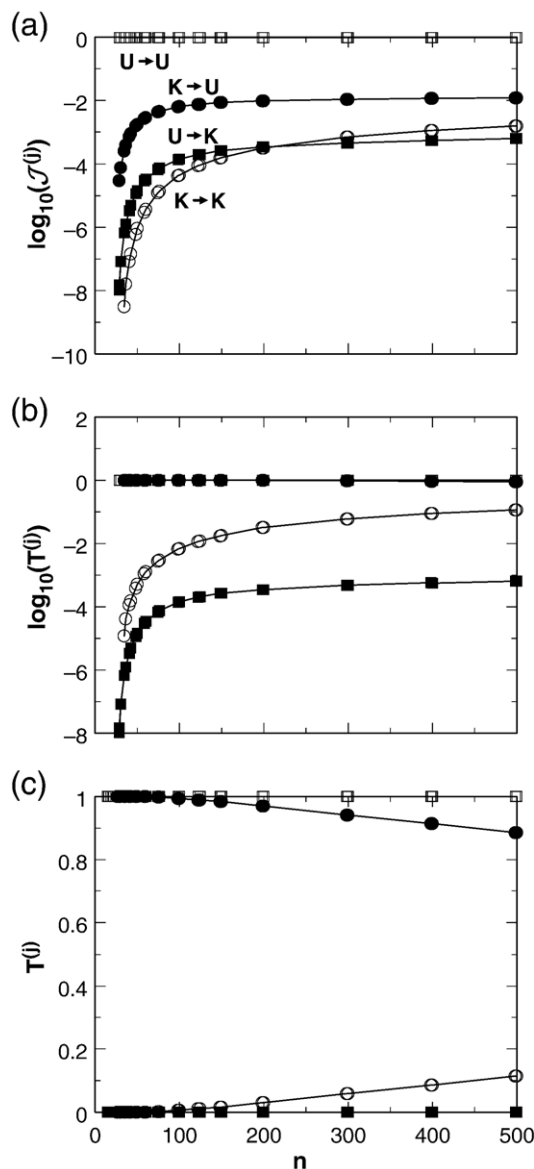
<sup>a</sup> It is important to note that although the conformational enumeration and Monte Carlo sampling part of our computation in obtaining  $\mathcal{J}_{K \rightarrow U}^{(j)}$  and  $\mathcal{J}_{U \rightarrow K}^{(j)}$  was conducted under conditions of topological equilibrium, the transition probabilities  $T_{K \rightarrow U}^{(j)}$  and  $T_{U \rightarrow K}^{(j)}$  in equation (5) are generally applicable and independent of any assumption of topological equilibrium. By definition, these quantities involve averaging over conformations only within the knot state ( $T_{K \rightarrow U}^{(j)}$ ) or only within the unknot state ( $T_{U \rightarrow K}^{(j)}$ ), but not both.

approach because  $\sim 97\%$  of nontrivial knots are trefoils in conformations without a preformed juxtaposition for the largest loop size  $n=500$  in the present study. Topological complexity is higher among  $n=500$  knotted loops with a preformed hooked juxtaposition (I); but still  $\sim 91\%$  are trefoils. The corresponding trefoil percentages are even higher for smaller loop sizes (Table 1).

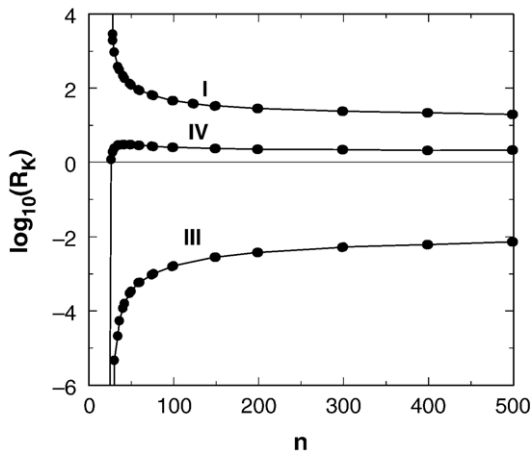
**Juxtaposition-driven topological transitions and knot reduction**

Figure 5 applies the above formulation to analyze knot reduction by segment passage at the hooked juxtaposition (I) as a function of loop size  $n$ . The quantities  $\mathcal{J}_{U \rightarrow U}^{(j)}$ ,  $\mathcal{J}_{K \rightarrow U}^{(j)}$ ,  $\mathcal{J}_{U \rightarrow K}^{(j)}$ , and  $\mathcal{J}_{K \rightarrow K}^{(j)}$  are plotted in Figure 5(a). Almost all segment passages take an unknot to an unknot ( $\mathcal{J}_{U \rightarrow U}^{(j)} \approx 1$ ) because, for the loop sizes we have examined, an overwhelming majority of the conformations are not knotted. The general trend of dependence on  $n$  of the other three  $\mathcal{J}^{(j)}$  values are similar to the  $p_K|_I$  trend for the hooked juxtaposition in Figure 2. However, Figure 5 shows that it is much more likely, by approximately one order of magnitude or more, for a segment passage at a hooked juxtaposition to change a knot to an unknot than either changing an unknot to a knot or failing to unknot a knot ( $\mathcal{J}_{K \rightarrow U}^{(j)} \gg \mathcal{J}_{U \rightarrow K}^{(j)}$  and  $\mathcal{J}_{K \rightarrow U}^{(j)} \gg \mathcal{J}_{K \rightarrow K}^{(j)}$ ). The power of segment passage at a hooked juxtaposition to unknot is shown even more clearly by the transition probabilities in Figure 5(b) and (c). These results show that if a conformation is initially unknotted, it is practically certain that it would remain unknotted after a segment passage at a hooked juxtaposition ( $T_{U \rightarrow U}^{(j)} \approx 1$ , and thus  $T_{U \rightarrow K}^{(j)} \approx 0$ ). On the other hand, if a conformation is initially knotted, there is a very high probability that it would be unknotted by a segment passage at a hooked juxtaposition. This is practically a certainty for small loops, and this probability decays only very slowly with increasing loop size  $n$ . Even for  $n=500$ , the unknotting transition probability  $T_{K \rightarrow U}^{(j)} \approx 0.9$ . In other words, there is only a small probability  $T_{K \rightarrow K}^{(j)} (= 1 - T_{K \rightarrow U}^{(j)})$  that a knotted conformation with  $n \leq 500$  would remain knotted after segment passage at a hooked juxtaposition.

The data in Figure 5 can now be used in equation (7) to compute the knot reduction factor  $R_K$  as a function of loop size  $n$  for the hooked (I), free non-planar (III), and half-hooked (IV) juxtapositions (Figure 6). Consistent with intuition, segment passage at a hooked juxtaposition reduces the knot population substantially. In contrast, segment passage at a free juxtaposition increases the knot population by approximately two orders of magnitude relative to that at equilibrium. Segment passage at the half-hooked juxtaposition also reduces the knot population for  $n \geq 26$ , but the knot reduction factor  $R_K$  is smaller than that of the hooked juxtaposition—by approximately one order of magnitude for loop size  $n=500$ , for example. For smaller loops, the differences in  $R_K$  among the three juxtapositions are



**Figure 5.** (a) Simulated probabilities  $\mathcal{J}^{(j)}$  of various interconversions between topological states upon virtual segment passage at the hooked juxtaposition (I) of a conformation, as function of loop size  $n$ . Unknot to unknot ( $U \rightarrow U$ ,  $\square$ ), unknot to knot ( $U \rightarrow K$ ,  $\blacksquare$ ), knot to knot ( $K \rightarrow K$ ,  $\circ$ ), and knot to unknot ( $K \rightarrow U$ ,  $\bullet$ ) are shown. The difference between  $U \rightarrow K$  and  $K \rightarrow U$  probabilities (filled symbols) dictates knot reduction. (b) Transition probabilities  $T^{(j)}$  when the initial conformation before segment passage is in the designated initial topological state. For example,  $T_{K \rightarrow U}^{(j)}$  gives the conditional probability of changing a knot to an unknot conformation provided the initial conformation is a knot. (c) Same transition probabilities plotted using a linear scale to show clearly the difference between  $T^{(j)}$  values for  $U \rightarrow U$  and  $K \rightarrow U$ . Results presented in (a)–(c) for  $n \leq 30$  are obtained by exact enumeration; whereas results for  $n \geq 30$  are obtained by Monte Carlo simulation, with the number of attempted chain moves for each datapoint varying from  $1.2 \times 10^{10}$  to  $1.8 \times 10^{10}$ . (Both exact enumeration and Monte Carlo sampling are used here and in Figure 6 for  $n=30$  with excellent agreement between the two methods.)



**Figure 6.** Loop size dependence of the knot reduction factor  $R_K$  for the hooked (I), free nonplanar (III), and half-hooked (IV) juxtapositions. Curves through the datapoints are merely a guide for the eye. Results for  $n \leq 30$  are obtained by exact enumeration, whereas results for  $n \geq 30$  are obtained by Monte Carlo simulation. The number of attempted chain moves for each Monte Carlo datapoint varies from  $1.2 \times 10^{10}$  to  $1.8 \times 10^{10}$ . The smallest  $n$  for a conformation with a juxtaposition I, III, and IV to be a knot is, respectively,  $n=26$ , 30, and 26. The corresponding minimum  $n$  for a finite  $\log R_K$  value is  $n=28$ , 30, and 26. For juxtaposition I,  $T_{K \rightarrow U}^{(j)} > 0$  but  $T_{U \rightarrow K}^{(j)} = 0$  when  $n=26$ , thus  $\log R_K \rightarrow \infty$ . For juxtaposition III with  $n=24$ , 26, and 28, and juxtaposition IV with  $n=24$ ,  $T_{U \rightarrow K}^{(j)} > 0$  but a knot to unknot transition is impossible; hence  $\log R_K \rightarrow -\infty$ . For juxtaposition IV,  $\log_{10} R_K \approx 0.079$  for  $n=26$  and attains a maximum value of  $\approx 0.48$  around  $n=40-50$ .

larger. Remarkably, however, the  $R_K$  values are quite stable for  $n > 200$ , and vary only slightly through the largest loop size  $n=500$  we have studied.

We have also considered 5mer-on-3mer juxtapositions (data not plotted). The shortened version of the half-hooked juxtaposition (IV) that possesses a three-bead straight segment instead of a five-bead straight segment has the highest  $R_K$  value among all 5mer-on-3mer juxtapositions. However, its  $R_K$  is smaller than that of the 5mer-on-5mer half-hooked juxtaposition (IV). For example, for  $n=100$ , the  $R_K$  values for the 5mer-on-3mer and 5mer-on-5mer versions of the half-hooked juxtapositions are 1.69 and 2.55, respectively. The corresponding  $R_K$  values for  $n=500$  are 1.60 and 2.15.

At this juncture, it is instructive to compare the steady-state knot reduction factor in our model to that deduced from the “active bending model” of Vologodskii and coworkers.<sup>18,19</sup> The active bending model stipulates that the topoisomerase first introduces a sharp turn along the DNA chain at the binding site, forming a hairpin-shaped segment. Then it waits for another part of the DNA chain to drift into the proximity of the hairpin, and drives segment passage only in one direction, in a manner similar to the segment passage operation at our juxtaposition (IV). As pointed out above, this proposed mechanism is physically different from that of Buck and Zechiedrich,<sup>25</sup> who envision the

topoisomerase to act on pre-existing hooked, and to a lesser extent, half-hooked juxtapositions. Nonetheless, mathematically, our formulation for computing steady-state knot population is quite similar to that in the active bending model because both formulations use simple rate equations to account for population changes driven by segment passages.

Because the active bending model proposes that DNA conformational distribution is altered by topoisomerase binding before segment passage, conformational properties of DNA ensembles with the topoisomerase-induced hairpin have to enter into the calculation of the steady-state knot population. In particular, the unknot and knot conformational populations constrained to contain the given hairpin (i.e., half-hooked single segment of a potential juxtaposition), denoted here as  $P_U^{[j/2]}$  and  $P_K^{[j/2]}$  respectively, have to be determined. This consideration is not necessary in our formulation. A simple analysis (details not shown) indicates that the knot reduction factor in the previous studies<sup>18,19</sup> is equal to our  $R_K$  in equation (7) multiplied by a factor of  $[P_U^{[j/2]}/P_K^{[j/2]}]/[(P_U)_{\text{eq}}/(P_K)_{\text{eq}}]$  if the juxtaposition geometry before segment passage in the two proposed mechanisms are identical. This relationship implies that although the knot reduction factors in the two models are different, practically they can be similar because  $P_U^{[j/2]}/P_K^{[j/2]} \approx (P_U)_{\text{eq}}/(P_K)_{\text{eq}}$ . For instance, for loop size  $n=100$  in our model,  $P_U^{[j/2]}/P_K^{[j/2]} = 1.12 \times 10^4$  and  $(P_U)_{\text{eq}}/(P_K)_{\text{eq}} = 1.16 \times 10^4$ . Because segment passages in the active bending model mechanism<sup>18,19</sup> occur at a juxtaposition geometry similar to that of our half-hooked juxtaposition (IV) (see above), if one applied the active bending model mechanism to our lattice model, the resulting steady-state knot reduction factor would be very similar to our  $R_K$  in Figure 6 for juxtaposition IV. Consistent with earlier findings,<sup>18,19</sup> segment passages at the half-hooked juxtaposition (IV) reduce knot population ( $\log R_K > 0$ ), but our results also show that juxtaposition IV is far less effective in driving unknotting than the hooked juxtaposition (I).

### Knot reduction by segment passage correlates with juxtaposition hookedness

Figure 7 extends our analysis of knot reduction factors to encompass all 680 5mer-on-5mer juxtaposition geometries that permit virtual segment passages. A conspicuous feature of this comprehensive survey is that most of the datapoints in the scatter plots lie below the horizontal dashed lines for  $R_K=1$  ( $\log R_K=0$ ), indicating that segment passage at a majority of juxtaposition geometries leads to a knot population increase ( $\log R_K < 0$ ), rather than a decrease. Only 7–15% of juxtaposition geometries can drive unknotting ( $\log R_K > 0$ ). This observation implies that, to achieve unknotting by segment passage, a rather stringent selection of juxtaposition geometry is necessary.

Figure 7 shows that the largest knot reduction among the 680 juxtapositions is achieved by the

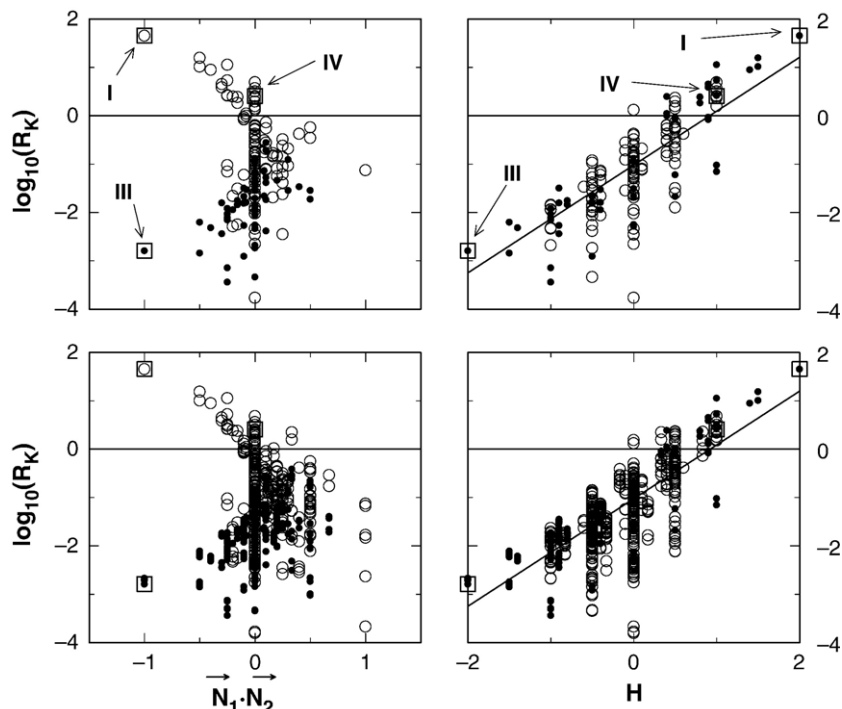


**Figure 7.** Correlations between the knot reduction factor  $R_K$  and juxtaposition geometries with well-defined virtual segment passages (cf. Figure 4), for loops of size  $n=100$ . The meaning of the symbols is the same as that in Figure 3. Upper panels: 175 juxtapositions that satisfy a stringent segment-passage criterion, with a crossing and admitting a central-bead swap, as for the examples in Figure 4(a). Lower panels: All 680 juxtapositions that have a crossing, as for the examples in Figure 4(a)–(c). Results are obtained from Monte Carlo sampling using  $4 \times 10^8$  attempted chain moves for each datapoint. Horizontal dashed lines mark the  $R_K=1$  level; virtual segment passages of the juxtapositions at this level will not change the knot/unknot population ratio from that of the equilibrium value. Only 27/175=15.4% and 45/680=6.6% of the juxtapositions in the upper and

lower panels, respectively, have  $R_K > 1$ . Dotted lines are least-squares fits. The Pearson correlation coefficients are  $r=0.88$  (upper),  $0.87$  (lower) for  $\vec{N}_1 \cdot \vec{N}_2 < 0$ ,  $r=0.72$  (upper),  $0.62$  (lower) for  $\vec{N}_1 \cdot \vec{N}_2 > 0$ , and  $r=0.81$  (upper),  $0.71$  (lower) overall.

hooked juxtaposition (I), which, at  $H=2$ , has the most hooked geometry. In comparison, although the free nonplanar juxtaposition (III), which has  $H=-2$ , does not have the smallest  $R_K$ ; its  $R_K$  value is lower than that of all except a few juxtapositions. The half-hooked juxtaposition (IV) has an intermediate hook parameter  $H=1$  that is closer to the hooked juxtaposition than to the free juxtaposition and a knot reduction factor  $R_K > 1$  ( $\log R_K > 0$ ) that is substantially lower than that of the hooked juxtaposition. Interestingly, for these three juxtapositions,  $\log R_K$  varies essentially linearly with  $H$ . Furthermore, our comprehensive survey reveals that this contrast among the hooked (I), free nonplanar (III), and half-hooked (IV) juxtapositions is part of a larger pattern of behavior that appears to govern the relationship between knot reduction and juxtaposition hookedness. Here, the right panels of Figure 7 indicate that, despite the datapoints being somewhat scattered, there is good correlation between the logarithmic knot reduction factor and  $H$  (see figure caption). The  $\log R_K$  versus  $H$  correlation is particularly strong among juxtapositions with their two segments curving away from each other ( $\vec{N}_1 \cdot \vec{N}_2 < 0$ ), which include both the hooked and free juxtapositions. As far as a general positive correlation between knot reduction effectiveness and juxtaposition hookedness is concerned, this trend is also in line with the fact that the variation of  $H$  among  $\vec{N}_1 \cdot \vec{N}_2 < 0$  juxtapositions captures more closely one’s intuitive sense of hookedness than the variation of  $H$  in general (cf. Figure 8 of Liu et al.<sup>30</sup>).

The scatter in the  $\log R_K$  versus  $H$  plots in Figure 7 (right) is markedly reduced relative to that in the  $\log f_K$  versus  $H$  plot in Figure 3(c). At least two

factors may be pertinent to the reduced scatter. First, some of the juxtapositions in Figure 3 that contributed to the wide spread in  $f_K$  lack a crossing. For example, the two  $H=2$  datapoints in Figure 3 that have significantly lower  $f_K$  than that of the hooked (I) are from juxtapositions without a crossing, and thus are not considered in the  $R_K$  analysis. Second,  $R_K$  provides different information from that of  $f_K$ . Among juxtapositions with a crossing, the correlation between  $\log f_K$  and  $\log R_K$  is not strong (Pearson coefficient  $r \approx 0.5$ , detailed data not shown). For example, even though the  $f_K$  values of two juxtapositions, each with a crossing, are slightly higher than that of the hooked (I) in Figure 3(b) and (c), the  $R_K$  of the hooked (I) clearly surpasses that of all other juxtapositions in Figure 7.

Two additional considerations are noteworthy in the interpretation of our model predictions. First, our conformational simulations are performed for juxtapositions with a positive crossing (Table 1). As such, they model directly segment passages at positive juxtapositions. Nonetheless, for highly symmetric geometries such as that of the hooked (I), free nonplanar (III), and half-hooked (IV) juxtapositions, the  $R_K$  values we have computed apply also to the situation in which segment passages are carried out at these juxtapositions without regard to the sign of the crossing. Second, the high  $R_K$  of the hooked juxtaposition and the diversity in  $R_K$  values among different juxtapositions (Figure 7) decrease with increasing loop size  $n$  (Figure 6). But for  $n > 200$ , these decreases are very gradual. The knot reduction factor  $R_K$  remains substantial at  $n=500$  and there is no obvious reason to assume that it will approach

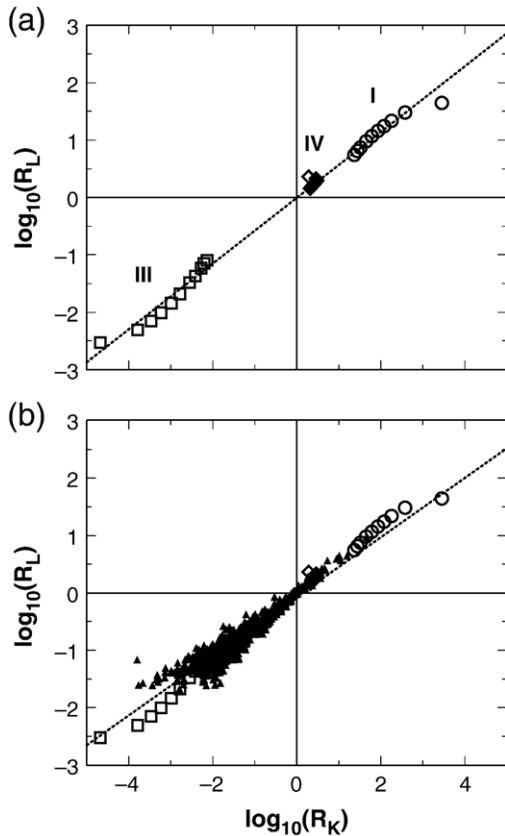


**Figure 8.** Correlations between the knot reduction factor  $R_K$  and the link reduction factor  $R_L$ . (a) Only juxtaponitions I (○), III (□), and IV (◇) with loop sizes varying from  $n=26$  to  $n=500$  are analyzed (cf. Figure 6). Results are obtained using Monte Carlo sampling, with the number of attempted chain moves for each single-loop system (for  $R_K$ ) ranging from  $1.2 \times 10^{10}$  to  $1.8 \times 10^{10}$ , and for each two-loop system (for  $R_L$ ) ranging from  $3 \times 10^9$  to  $1.8 \times 10^{10}$ . (b) Knot and link reduction factors for all 680 juxtaponitions with a crossing (same as those in the lower panels of Figure 7) and loop size  $n=100$  are plotted as solid triangles (▲) overlaid onto data from (a). The extensive set of results was obtained from Monte Carlo sampling using  $4 \times 10^8$  and  $6 \times 10^8$  attempted chain moves, respectively, for each single- and two-loop system. The horizontal and vertical dashed lines mark the  $R_K=1$  and  $R_L=1$  levels, respectively. Dotted straight lines are least-squares fits to the datapoints. The corresponding Pearson correlation coefficients are (a)  $r=0.997$ , (b)  $r=0.947$  for the solid triangles, alone, and  $r=0.962$  for all  $R_K$  and  $R_L$  values plotted.

unity ( $\log R_K \rightarrow 0$ ) even for much larger  $n$ . As for the decatenation case,<sup>30</sup> our results suggest strongly that the local geometry and sterics of a given juxtaposition always impose an intrinsic conformational bias with global topological consequences that cannot be abolished by increasing loop size.

### Unknotting and decatenating effects of a juxtaposition are related

Experiments indicate that the discrimination of a type-2 topoisomerase to unknot is correlated with its

discrimination to decatenate.<sup>17</sup> Figure 8 examines the correlation between the knot reduction factor  $R_K$  and a similarly defined link reduction factor  $R_L$  that we computed here by applying virtual segment passage operations to the results from our previous catenation/decatenation study.<sup>30</sup> Figure 8(a) considers the effects of segment passages at the three special juxtapositions I, III, and IV on one- and two-loop systems of different sizes  $n$ . Figure 8(b) extends the comparison to include unknotting and decatenation data on loops of size  $n=100$  for all 5mer-on-5mer juxtaposition geometries that permit segment passage. There is a striking correlation between  $\log R_K$  and  $\log R_L$  in both cases.

To relate our knot and link reduction factors to the ratio of equilibrium to steady-state fractions of knots ( $R_{kn}$ ) and catenanes ( $R_{cat}$ ) defined in the experimental study of Rybenkov *et al.*,<sup>17</sup> it is straightforward to show that:

$$R_{kn} = \frac{(P_K)_{eq}}{(P_K)_{st}} = \frac{R_K + [(P_K)_{eq}/(P_U)_{eq}]}{1 + [(P_K)_{eq}/(P_U)_{eq}]} \quad (8)$$

and that an analogous relationship holds for  $R_{cat}$  and  $R_L$ . Because the equilibrium knot to unknot ratio  $[(P_K)_{eq}/(P_U)_{eq}] \ll 1$  for our model loop sizes and also for the plasmid DNA used in the experiments:<sup>17</sup>

$$R_{kn} \approx R_K \quad (9)$$

and thus we may compare the experimental  $R_{kn}$  with our model  $R_K$ .

Our model is highly simplified and coarse-grained. Nonetheless, the general trends exhibited in Figure 8 are in remarkable agreement with existing experimental data. First,  $R_K$  of the hooked juxtaposition (I) decreases with increasing loop size  $n$  in our model. Provided that type-2 topoisomerases act on certain types of hooked juxtapositions,<sup>25,30</sup> this prediction is consistent with the finding<sup>17</sup> that the action of (type-2) topoisomerase IV from *Escherichia coli* on the 7 kb (kilobase) pAB4 plasmid DNA leads to  $R_{kn} \approx 90$ , whereas the action of the same topoisomerase on the larger 10 kb P4 DNA results in a smaller  $R_{kn} \approx 50$ . Second, the strong correlation between the experimental  $\log R_{kn}$  and  $\log R_{cat}$  resulting from the action of type-2 topoisomerases from different organisms on the 7 kb plasmid DNA<sup>17</sup> may be explained by the strong correlation between  $\log R_K$  and  $\log R_L$  in Figure 8(b). In this regard, if one assumes that  $R_{cat} \approx R_L$ , our model prediction of the scaling relationship  $R_K \approx (R_L)^2$  (Figure 8(b)) is in reasonable agreement with the  $R_{kn} \approx (R_{cat})^{1.6}$  reported in Figure 3(a) of Rybenkov *et al.*<sup>17</sup> Third, the experimental  $R_{kn} \approx 90$  and  $R_{cat} \approx 16$  for the pAB4 DNA<sup>17</sup> are within the ranges of  $R_K$  and  $R_L$  values, respectively, of our hooked juxtaposition (I) for the various loop sizes we examined. Interestingly, the corresponding  $R_K$  and  $R_L$  values of the half-hooked juxtaposition (IV) show little variation with loop size for  $n \leq 500$ , and are too small to match the experimental  $R_{kn}$  and  $R_{cat}$

values. Although further analysis is necessary, this model result should be relevant in assessing the viability of the active bending model.<sup>18,19</sup> Indeed, the active bending model is insufficient for producing the experimentally observed level of unknotting.<sup>21</sup> For example, an application of that model to a 7 kb DNA<sup>19</sup> yielded a knot reduction factor  $\sim 10$  ( $=P_k/(C_k/C_u)$ ) in Table 1 of Vologodskii et al.<sup>19</sup><sup>b</sup>, and a link reduction factor  $\sim 4$ ; both are substantially lower than the corresponding values of 90 and 16 achieved experimentally.<sup>17</sup>

## Concluding Remarks

An open question in understanding how type-2 topoisomerases perform their crucial biological functions has been how does an enzyme that is much smaller than its DNA substrate preferentially decatenate or unknot rather than catenate or knot DNA. Here, as in our previous work on decatenation,<sup>30</sup> we address this fundamental question in general terms. The extension from decatenation<sup>30</sup> to unknotting represents an important step forward because while the special role of hooked juxtapositions in decatenation may be grasped intuitively by considering catenanes of perfect circles,<sup>25</sup> the special role of hooked juxtaposition in unknotting is less straightforward. Our work has shown that discriminatory topological information is embodied in local juxtaposition geometries such that selective segment passages at hooked juxtapositions can be a highly successful strategy for disentangling, rather than entangling, both catenanes and knots.

Whether type-2 topoisomerases have made use of the statistical mechanical principles uncovered by our model simulations is a question that can only be answered by further experimental investigation. Nonetheless, our work has highlighted a remarkable physical trend. Our model predictions with regard to the magnitude of type-2 topoisomerase-driven unknotting and the near-perfect correlation between logarithmic decatenating and unknotting factors are in excellent agreement with existing experiments. Future prospects are exciting. The juxtaposition-centric framework, and the general predictions of our model should guide experimental work to

<sup>b</sup> The steady-state knot reduction factor relative to that at topological equilibrium in the active bending model should be defined as the ratio of the equilibrium probability of knotting,  $P_k=0.014$ , to the steady-state fraction of knots,  $C_k/(C_k+C_u)\approx(C_k/C_u)=0.0014$  for the "hairpin G segment" process in that model. The knot/unknot ratio of 0.020, which is approximately equal to the knot probability, for the "straight G segment" process<sup>19</sup> should not be used instead of  $P_k$ . Indeed, the fact that  $P_k<0.020$  implies that the "straight G segment" process in Vologodskii et al.<sup>19</sup> increases knotting relative to topological equilibrium. This trend is consistent with our finding that the 5mer-on-5mer juxtaposition with two straight segments at a 90° cross angle ( $\vec{N}_1 \cdot \vec{N}_2, H=0$ ) also increases knotting, with  $R_K=0.18$  for  $n=100$ .

contribute to the deciphering of type-2 topoisomerase action.

## Acknowledgements

We dedicate this work to the memory of Dr. Nick Cozzarelli. We thank him for countless discussions and advice and his invaluable contributions to the field. We are grateful to Drs. De Witt L. Sumners and Gregory R. Buck for helpful discussions. Z.L. was supported in part by a Premier's Research Excellence Award (Ontario) to H.S.C. J.K.M. was supported by a pre-doctoral fellowship from the Program in Mathematics and Molecular Biology at Florida State University with funding from the National Science Foundation and the Burroughs Wellcome Fund Interfaces Program. Financial support for this research was provided also by National Institutes of Health grant RO1 AI054830 and the Burroughs Wellcome Fund to E.L.Z. The research of H.S.C. has been supported partly by the Canadian Institutes of Health Research (grant MOP-15323), the Canada Foundation for Innovation, and the Ontario Innovation Trust. H.S.C. holds a Canada Research Chair in Proteomics, Bioinformatics and Functional Genomics.

## References

1. Frisch, H. L. & Wasserman, E. (1961). Chemical topology. *J. Am. Chem. Soc.* **83**, 3789–3795.
2. Delbrück, M. (1962). Knotting problems in biology. In *Mathematical Problems in the Biological Sciences* (Proceedings of Symposia in Applied Mathematics, Vol. 14), pp. 55–63, American Mathematical Society, Providence, Rhode Island, USA.
3. Shishido, K., Komiyama, N. & Ikawa, S. (1987). Increased production of a knotted form of plasmid pBR322 DNA in *Escherichia coli* DNA topoisomerase mutants. *J. Mol. Biol.* **195**, 215–218.
4. Martin-Parras, L., Lucas, I., Martinez-Robles, M. L., Hernandez, P., Krimer, D. B., Hyrien, O. & Schwartzman, J. B. (1998). Topological complexity of different populations of pBR322 as visualized by two-dimensional agarose gel electrophoresis. *Nucleic Acids Res.* **26**, 3424–3432.
5. Podtelezhnikov, A. A., Cozzarelli, N. R. & Vologodskii, A. V. (1999). Equilibrium distributions of topological states in circular DNA: interplay of supercoiling and knotting. *Proc. Natl Acad. Sci. USA*, **96**, 12974–12979.
6. Wang, J. C. (1996). DNA topoisomerases. *Annu. Rev. Biochem.* **65**, 635–692.
7. Champoux, J. J. (2001). DNA topoisomerases: structure, function, and mechanism. *Annu. Rev. Biochem.* **70**, 369–413.
8. Nitiss, J. & Wang, J. C. (1988). DNA topoisomerase-targeting antitumor drugs can be studied in yeast. *Proc. Natl Acad. Sci. USA*, **85**, 7501–7505.
9. Khodursky, A. B., Zechiedrich, E. L. & Cozzarelli, N. R. (1995). Topoisomerase-IV is a target of quinolones in *Escherichia coli*. *Proc. Natl Acad. Sci. USA*, **92**, 11801–11805.

10. Li, T. K. & Liu, L. F. (2001). Tumor cell death induced by topoisomerase-targeting drugs. *Annu. Rev. Pharmacol. Toxicol.* **41**, 53–77.
11. Gruger, T., Nitiss, J. L., Maxwell, A., Zechiedrich, E. L., Heisig, P., Seeber, S. *et al.* (2004). A mutation in *Escherichia coli* DNA gyrase conferring quinolone resistance results in sensitivity to drugs targeting eukaryotic topoisomerase II. *Antimicrob. Agents Chemother.* **48**, 4495–4504.
12. Wang, J. C. (1971). Interaction between DNA and an *Escherichia coli* protein *ω*. *J. Mol. Biol.* **55**, 523–533.
13. Sikorav, J. L. & Jannink, G. (1994). Kinetics of chromosome condensation in the presence of topoisomerases – a phantom chain model. *Biophys. J.* **66**, 827–837.
14. Pulleyblank, D. E., Shure, M., Tang, D., Vinograd, J. & Vosberg, H. P. (1975). Action of nicking-closing enzyme on supercoiled and nonsupercoiled closed circular DNA: formation of a Boltzmann distribution of topological isomers. *Proc. Natl Acad. Sci. USA*, **72**, 4280–4284.
15. Shaw, S. Y. & Wang, J. C. (1993). Knotting of a DNA chain during ring-closure. *Science*, **260**, 533–536.
16. Rybenkov, V. V., Vologodskii, A. V. & Cozzarelli, N. R. (1997). The effect of ionic conditions on the conformations of supercoiled DNA. 2. Equilibrium catenation. *J. Mol. Biol.* **267**, 312–323.
17. Rybenkov, V. V., Ullsperger, C., Vologodskii, A. V. & Cozzarelli, N. R. (1997). Simplification of DNA topology below equilibrium values by type II topoisomerases. *Science*, **227**, 690–693.
18. Vologodskii, A. (1998). Maxwell demon and topology simplification by type II topoisomerases. In *RECOMB 98: Proceedings of the Second Annual International Conference on Computational Molecular Biology*, pp. 266–269, Association for Computing Machinery, New York, USA.
19. Vologodskii, A. V., Zhang, W., Rybenkov, V. V., Podtelezchnikov, A. A., Subramanian, D., Griffith, J. D. & Cozzarelli, N. R. (2001). Mechanism of topology simplification by type II DNA topoisomerases. *Proc. Natl Acad. Sci. USA*, **98**, 3045–3049.
20. Wang, J. C. & Gjaever, G. N. (1988). Action at a distance along a DNA. *Science*, **240**, 300–304.
21. Yan, J., Magnasco, M. O. & Marko, J. F. (1999). A kinetic proofreading mechanism for disentanglement of DNA by topoisomerases. *Nature*, **401**, 932–935.
22. Yan, J., Magnasco, M. O. & Marko, J. F. (2001). Kinetic proofreading can explain the suppression of supercoiling of circular DNA molecules by type-II topoisomerases. *Phys. Rev. E*, **63**, 031909.
23. Trigueros, S., Salceda, J., Bermudez, I., Fernández, X. & Roca, J. (2004). Asymmetric removal of supercoils suggests how topoisomerase II simplifies DNA topology. *J. Mol. Biol.* **335**, 723–731.
24. Maxwell, A., Costenaro, L., Mittelheiser, S. & Bates, A. D. (2005). Coupling ATP hydrolysis to DNA strand passage in type IIA DNA topoisomerases. *Biochem. Soc. Trans.* **33**, 1460–1464.
25. Buck, G. R. & Zechiedrich, E. L. (2004). DNA disentangling by type-2 topoisomerases. *J. Mol. Biol.* **340**, 933–939.
26. Zechiedrich, E. L. & Osheroff, N. (1990). Eukaryotic topoisomerases recognize nucleic acid topology by preferentially interacting with DNA crossovers. *EMBO J.* **9**, 4555–4562.
27. Corbett, K. D., Schoeffler, A. J., Thomsen, N. D. & Berger, J. M. (2005). The structural basis for substrate specificity in DNA topoisomerase IV. *J. Mol. Biol.* **351**, 545–561.
28. Schoeffler, A. J. & Berger, J. M. (2005). Recent advances in understanding structure–function relationships in the type II topoisomerase mechanism. *Biochem. Soc. Trans.* **33**, 1465–1470.
29. Germe, T. & Hyrien, O. (2005). Topoisomerase II–DNA complexes trapped by ICRF-193 perturb chromatin structure. *EMBO Rep.* **6**, 729–735.
30. Liu, Z., Zechiedrich, E. L. & Chan, H. S. (2006). Inferring global topology from local juxtaposition geometry: interlinking polymer rings and ramifications for topoisomerase action. *Biophys. J.* **90**, 2344–2355.
31. Zechiedrich, E. L. & Cozzarelli, N. R. (1995). Roles of topoisomerase IV and DNA gyrase in DNA unlinking during replication in *Escherichia coli*. *Genes Dev.* **9**, 2859–2869.
32. Zechiedrich, E. L., Khodursky, A. B. & Cozzarelli, N. R. (1997). Topoisomerase IV, not gyrase, decatenates products of site-specific recombination in *Escherichia coli*. *Genes Dev.* **11**, 2580–2592.
33. Randall, G. L., Pettitt, B. M., Buck, G. R. & Zechiedrich, E. L. (2006). Electrostatics of DNA–DNA juxtapositions: consequences for type II topoisomerase function. *J. Phys., Condens. Matter*, **18**, S173–S185.
34. Deibler, R. W., Rahmati, S. & Zechiedrich, E. L. (2001). Topoisomerase IV, alone, unknots DNA in *E. coli*. *Genes Dev.* **15**, 748–761.
35. Orr, W. J. C. (1947). Statistical treatment of polymer solutions at infinite dilution. *Trans. Faraday Soc.* **43**, 12–27.
36. Domb, C. (1969). Self avoiding walks on lattices. *Adv. Chem. Phys.* **15**, 229–259.
37. Taketomi, H., Ueda, Y. & Gö, N. (1975). Studies on protein folding, unfolding and fluctuations by computer simulation. 1. The effect of specific amino acid sequence represented by specific inter-unit interactions. *Int. J. Pept. Protein Res.* **7**, 445–459.
38. Chan, H. S. & Dill, K. A. (1989). Intrachain loops in polymers: effects of excluded volume. *J. Chem. Phys.* **90**, 492–509 [Errata: **96**, 3361 (1992); **107**, 10353 (1997)].
39. Chan, H. S. & Dill, K. A. (1990). Origins of structure in globular proteins. *Proc. Natl Acad. Sci. USA*, **87**, 6388–6392.
40. Shakhnovich, E. I., Farztdinov, G., Gutin, A. M. & Karplus, M. (1991). Protein folding bottlenecks: a lattice Monte Carlo simulation. *Phys. Rev. Letters*, **67**, 1665–1668.
41. Leopold, P. E., Montal, M. & Onuchic, J. N. (1992). Protein folding funnels: a kinetic approach to the sequence–structure relationship. *Proc. Natl Acad. Sci. USA*, **89**, 8721–8725.
42. Camacho, C. J. & Thirumalai, D. (1993). Kinetics and thermodynamics of folding in model proteins. *Proc. Natl Acad. Sci. USA*, **90**, 6369–6372.
43. Hinds, D. A. & Levitt, M. (1994). Exploring conformational space with a simple lattice model for protein structure. *J. Mol. Biol.* **243**, 668–682.
44. Bryngelson, J. D., Onuchic, J. N., Socci, N. D. & Wolynes, P. G. (1995). Funnel, pathways and the energy landscape of protein folding: a synthesis. *Proteins: Struct. Funct. Genet.* **21**, 167–195.
45. Shrivastava, I., Vishveshwara, S., Cieplak, M., Maritan, A. & Banavar, J. R. (1995). Lattice model for rapidly folding protein-like heteropolymers. *Proc. Natl Acad. Sci. USA*, **92**, 9206–9209.
46. Zarembinski, T. I., Kim, Y., Peterson, K., Christendat, D., Dharamsi, A., Arrowsmith, C. H. *et al.* (2003). Deep trefoil knot implicated in RNA binding found in an

- archaeobacterial protein. *Proteins: Struct. Funct. Genet.* **50**, 177–183.
47. Zhou, H.-X. (2004). Loops, linkages, rings, catenanes, cages, and crowders: entropy-based strategies for stabilizing proteins. *Acc. Chem. Res.* **37**, 123–130.
  48. Mallam, A. L. & Jackson, S. E. (2005). Folding studies on a knotted protein. *J. Mol. Biol.* **346**, 1409–1421.
  49. Wagner, J. R., Brunzelle, J. S., Forest, K. T. & Vierstra, R. D. (2005). A light-sensing knot revealed by the structure of the chromophore-binding domain of phytochrome. *Nature*, **438**, 325–331.
  50. Sumners, D. W. & Whittington, S. G. (1988). Knots in self-avoiding walks. *J. Phys. A*, **21**, 1689–1694.
  51. Soteros, C. E., Sumners, D. W. & Whittington, S. G. (1992). Entanglement complexity of graphs in  $Z^3$ . *Math. Proc. Camb. Phil. Soc.* **111**, 75–91.
  52. Orlandini, E., Tesi, M. C., Whittington, S. G., Sumners, D. W. & van Rensburg, E. J. J. (1994). The writhe of a self-avoiding walk. *J. Phys. A*, **27**, L333–L338.
  53. Yao, A., Matsuda, H., Tsukahara, H., Shimamura, M. K. & Deguchi, T. (2001). On the dominance of trivial knots among SAPs on a cubic lattice. *J. Phys. A*, **34**, 7563–7577.
  54. Moore, N. T., Lua, R. C. & Grosberg, A. Y. (2004). Topologically driven swelling of a polymer loop. *Proc. Natl Acad. Sci. USA*, **101**, 13431–13435.
  55. Szafron, M. L. & Soteros, C. E. (2005). The probability of knotting after a local strand passage in SAPs. *Abstr. Pap. Presented Am. Math. Soc.* **26**; 1004–62–177 ([http://www.ams.org/amsmtgs/2114\\_abstracts/1004-62-177.pdf](http://www.ams.org/amsmtgs/2114_abstracts/1004-62-177.pdf)).
  56. Hua, X., Nguyen, D., Raghavan, B., Arsuaga, J. & Vazquez, M. (2005). Random state transitions of knots: a first step towards modeling unknotting by type II topoisomerases. *Topology and its Applications*, accepted for publication ([http://math.berkeley.edu/~marie/Vazquez\\_topoII05.pdf](http://math.berkeley.edu/~marie/Vazquez_topoII05.pdf)).
  57. Cantor, C. R. & Schimmel, P. R. (1980). *Biophysical Chemistry*, Part III, pp. 979–1018, W. H. Freeman & Company, New York, USA.
  58. Freyd, P., Yetter, D., Hoste, J., Lickorish, W. B. R., Millett, K. & Ocneanu, A. (1985). A new polynomial invariant of knots and links. *Bull. Am. Math. Soc.* **12**, 239–246.
  59. Jenkins, R.J. (1989). *Knot Theory, Simple Weaves, and an Algorithm for Computing the HOMFLY Polynomial*. Master's thesis in Mathematics (Carnegie Mellon University, Pittsburgh, Pennsylvania, USA).
  60. Cromwell, P. (2004). *Knots and Links*, pp. 66–70, Cambridge University Press, Cambridge, UK.
  61. Rolfsen, D. (1976). *Knots and Links*. Publish or Perish Inc., Berkeley, California, USA.
  62. Saito, N. & Chen, Y. (1973). Statistics of a random coil chain in the presence of a point (two-dimensional case) or line (three-dimensional case) obstacle. *J. Chem. Phys.* **59**, 3701–3709.
  63. Chen, Y. (1981). Monte Carlo study of freely jointed ring polymers. II. The writhing number. *J. Chem. Phys.* **75**, 2447–2453.
  64. Koniaris, K. & Muthukumar, M. (1991). Self-entanglement in ring polymers. *J. Chem. Phys.* **95**, 2873–2881.
  65. Huang, J. Y. & Lai, P. Y. (2001). Crossings and writhe of flexible and ideal knots. *Phys. Rev. E*, **63**, 021506.
  66. Lai, P. Y. (2002). Dynamics of polymer knots at equilibrium. *Phys. Rev. E*, **66**, 021805.
  67. Dobay, A., Dubochet, J., Millett, K., Sottas, P. E. & Stasiak, A. (2003). Scaling behavior of random knots. *Proc. Natl Acad. Sci. USA*, **100**, 5611–5615.
  68. Buck, G. & Rawdon, E. J. (2004). Role of flexibility in entanglement. *Phys. Rev. E*, **70**, 011803.
  69. Flammini, A., Maritan, A. & Stasiak, A. (2004). Simulations of action of DNA topoisomerases to investigate boundaries and shapes of spaces of knots. *Biophys. J.* **87**, 2968–2975.
  70. Sheng, Y. J., Wu, C. N., Lai, P. Y. & Tsao, H. K. (2005). How knotting regulates the reversible intrachain reaction. *Macromolecules*, **38**, 2959–2965.
  71. Micheletti, C., Marenduzzo, D., Orlandini, E. & Sumners, D. W. (2006). Knotting of random ring polymers in confined spaces. *J. Chem. Phys.* **124**, 064903.
  72. Madras, N., Orlitsky, A. & Shepp, L. A. (1990). Monte Carlo generation of self-avoiding walks with fixed endpoints and fixed length. *J. Stat. Phys.* **58**, 159–183.
  73. Berg, B. & Foerster, D. (1981). Random paths and random surfaces on a digital computer. *Phys. Letters, Sect. B*, **106**, 323–326.
  74. de Carvalho, C. A., Caracciolo, S. & Fröhlich, J. (1983). Polymers and  $g|\Phi|^4$  theory in four dimensions. *Nucl. Phys., B*, **215**, 209–248.
  75. Alexander, J. W. (1928). Topological invariants of knots and links. *Trans. Am. Math. Soc.* **30**, 275–306.
  76. Harris, B. A. & Harvey, S. C. (1999). Program for analyzing knots represented by polygonal paths. *J. Comput. Chem.* **20**, 813–818.
  77. Vologodskii, A. V., Lukashin, A. V., Frank-Kamenetskii, M. D. & Anshelevich, V. V. (1974). The knot problem in statistical mechanics of polymer chains. *Sov. Phys. JETP*, **39**, 1059–1063.
  78. Diao, Y. (1993). Minimal knotted polygons on the cubic lattice. *J. Knot Theory Ramif.* **2**, 413–425.
  79. Pathria, R. K. (1980). *Statistical Mechanics*, p. 462, Pergamon Press, Oxford, UK.
  80. Chan, H. S. & Dill, K. A. (1993). Energy landscapes and the collapse dynamics of homopolymers. *J. Chem. Phys.* **99**, 2116–2127.

Edited by M. Levitt

(Received 13 April 2006; received in revised form 1 June 2006; accepted 3 June 2006)  
Available online 19 June 2006